Phonon dispersion of crystalline solids from the density-functional theory of freezing

Mangal C. Mahato,* H. R. Krishnamurthy,† and T. V. Ramakrishnan‡
Department of Physics, Indian Institute of Science, Bangalore 560 012, India
(Received 1 May 1991)

Phonon dispersion in solids is usually calculated starting from model interaction potentials. In this paper, we discuss an approach for calculating phonon energies in a crystalline solid close to melting, using the density-functional theory of freezing. This theory uses the (measured or calculated) direct correlation functions of the corresponding liquid close to freezing as input parameters. To illustrate the method we calculate phonon dispersion of solid argon close to its triple point, using two sets of experimental structure-factor data for liquid argon. We then discuss the phonon dispersion for a model solid with Lennard-Jones interaction potential, using a fit to the computer simulation results on the structure factor of the Lennard-Jones fluid. We also calculate the force constants of the solid from the liquid structure-factor data. Our calculation uses a parametrization of the solid density as a periodic isotropic Gaussian distribution centered at the corresponding crystal lattice sites, an approximation used by several authors previously in a variety of other contexts. The results that we obtain are qualitatively reasonable, but quantitatively they do not agree very well with the experimentally measured values: For example, at the zone boundaries our calculated phonon energies are larger by a factor of about 1.5. We discuss the reasons for the discrepancy, and how it can be overcome by improved calculations.

I. INTRODUCTION

In this paper we show how the density-functional theory of freezing can be used to calculate phonon frequencies in crystalline solids. The calculation of phonon spectra and their experimental determination are old problems in solid-state physics.[1] To set the stage for our study, we begin with a very brief review of current theories of phonon spectra.

Current theories of the phonon spectra of crystals have their origins in the well-known work of Born and von Kármán, a harmonic theory in which the potential-energy expansion is truncated up to terms that are quadratic in the displacements of the ions with respect to the lattice. The implementation of and improvement over the Born–von Kármán theory face two main difficulties: (1) It is not easy to determine the interionic potentials in various types of crystals (metallic, ionic, molecular, etc.). (2) It is nontrivial to include the effects of anharmonic terms at high temperatures where the ionic displacements from their equilibrium positions are not small. Since the early work of Born and von Kármán, many workers have tackled these and, as a result, the phonon spectra of nontransition metals[2] are fairly well understood in a microscopic way; however, for other types of solids, their description is more or less phenomenological.

A lot of work has been done on the lattice dynamics of rare-gas solids[3] because of their simplicity (both atomic and structural). For such solids, several realistic two-body interactions have been proposed.[3] Together with a three-body (Axilrod-Teller-Muto) potential, some of these two-body potentials explain various solid-state properties (e.g., elastic constants, etc.) fairly well. Quasiharmonic perturbation theory (where cubic and higher-order terms in the displacement are included perturbatively) and an improved self-consistent harmonic theory give phonon frequencies which compare excellently with experimental results at temperatures below about half the melting temperature.[3] Near the melting temperature, the vibrations have large amplitudes,[4] so the motion is strongly anharmonic. In addition, because of the hard-core potentials in these solids, short-range correlations become important. These problems have been addressed by Horner[5] and the theory has recently been put to actual calculation and compared with experimental results at temperatures near the melting point by Cowley and Horton.[6] The calculation of phonon frequencies compare very well with experimental results except near the zone boundaries. The discrepancies are supposed to arise because of uncertainties in the interaction potential used and multiphonon processes which have not been included in the calculation.

In this paper we propose a way of calculating phonon spectra of solids near melting, which, we believe, has the potential to overcome some of the complexities of conventional theories and can, in principle, circumvent the determination of phenomenological interaction potentials. Our theory uses the density-functional theory of freezing.[7,8] In this theory, given the structure factor of the liquid near its freezing point, we obtain a free-energy functional whose minimum characterizes the crystalline solid below the freezing point. Furthermore, we can calculate the free-energy cost of small deviations about the crystalline minimum and thus obtain phonon spectra for the solid.

We expect such a calculation of phonon spectra to give reasonable results since the density-functional theory of freezing has given good results for the freezing parameters of simple solids. Furthermore, it would have the following advantages over conventional approaches.

(1) Unlike conventional theories, the density-functional theory does not *require* phenomenological interionic potentials; instead, the *experimentally measured* structure factor of the liquid near the freezing point can be used. (For simple liquids, this structure factor can be obtained from approximate theories of liquids.)

(2) Some anharmonic corrections are automatically accounted for in the theory because the two-body direct correlation function (rather than a bare interionic potential) is used.

In order to account perturbatively for all anharmonic corrections within the density-functional theory, one would need higher n-body ($n>2$) correlation functions for the liquid which are not known.[9] In the illustrative calculations reported in this paper we have chosen the simplest functional, with n-body correlation functions set equal to zero for $n>2$. The results we obtain for the phonon spectrum of solid argon near its triple point using this functional, specific choices of inputs for the direct correlation function, and several simplifying assumptions, show qualitative but not quantitative agreement with experimental data. (Figure 1 shows a representative plot of our results and experimental data. Note the discrepancy of a factor of 1.5 at the zone boundary.) The velocities of sound that we find, while of the same order of magnitude as those measured experimentally, are also too large by roughly a factor of 2. We discuss the reasons for this discrepancy in detail and how it can be removed in Sec. V. The remaining part of this paper is organized as follows. In Sec. II we develop the density-functional theory description of phonon spectra. In Sec. III we discuss the structure factors that we use in our calculations. In Sec. IV we give the numerical results.

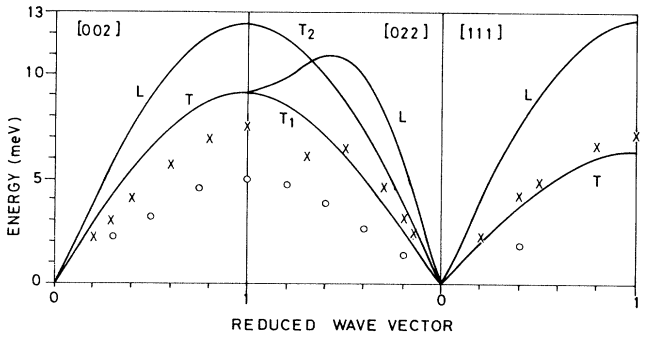

FIG. 1. Phonon-dispersion curves from our density-functional theory (solid lines) for crystalline argon near its melting point. For this figure we use $N_s=39$ and the structure-factor data of Yarnell *et al.* (Ref. 24). For comparison we show the experimental data of Eckert and Youngblood (Ref. 32); crosses (circles) are used for the longitudinal (transverse) modes. [In the (220) direction, these authors provide data for only one of the transverse modes, T_1.]

II. PHONON DISPERSION FROM THE DENSITY-FUNCTIONAL THEORY OF FREEZING

A. Density-functional theory of freezing

The grand free-energy functional W of a nonuniform liquid of density $\rho(\mathbf{r})$ can be expanded[7,8] about that for the uniform liquid of density ρ_0 as follows:

$$\beta(W-W_0)=\int d\mathbf{r}_1\rho(\mathbf{r}_1)\ln\left[\frac{\rho(\mathbf{r}_1)}{\rho_0}\right]-\int d\mathbf{r}_1[\rho(\mathbf{r}_1)-\rho_0]-\frac{1}{2!}\frac{1}{\rho_0}\int d\mathbf{r}_1\int d\mathbf{r}_2\,c^{(2)}(\mathbf{r}_1,\mathbf{r}_2)[\rho(\mathbf{r}_1)-\rho_0][\rho(\mathbf{r}_2)-\rho_0]$$
$$-\frac{1}{3!}\frac{1}{\rho_0^2}\int d\mathbf{r}_1\int d\mathbf{r}_2\int d\mathbf{r}_3\,c^{(3)}(\mathbf{r}_1,\mathbf{r}_2,\mathbf{r}_3)[\rho(\mathbf{r}_1)-\rho_0][\rho(\mathbf{r}_2)-\rho_0][\rho(\mathbf{r}_3)-\rho_0]-\cdots \quad (1)$$

where $c^{(n)}$ are the n-body direct correlation functions of the liquid evaluated at the liquid density ρ_0. For the calculations presented in this paper, we work with the simplest, Ramakrishnan-Yussouff (RY) functional,[7,8] where one neglects the correlation functions $c^{(n)}$ with $n\geq 3$ [and hence drop the superscript on the two-body direct correlation function $c^{(2)}(\mathbf{r}_1,\mathbf{r}_2)$]. The point is to find solutions $\rho(\mathbf{r})$ which minimize (1). The trivial solution is $\rho(\mathbf{r})=\rho_0$ corresponding to the liquid phase. The nontrivial solutions will correspond to nonuniform phases, e.g., the solid phase, where the $\rho(\mathbf{r})$ will have nonzero Fourier components.

We can describe the local density of the crystalline phase via the Fourier expansion

$$\rho(\mathbf{r})=\rho_0\left[1+\eta+\sum_{\mathbf{G}}\mu_{\mathbf{G}}e^{i\mathbf{G}\cdot\mathbf{r}}\right], \quad (2)$$

where $\mathbf{G}$'s are the reciprocal-lattice vectors that characterize the crystal. $\rho_0(1+\eta)$ is the density of solid η, the fractional density change on freezing, and the amplitudes $\{\mu_{\mathbf{G}}\}$ are the order parameters for this crystalline phase. They are determined by the condition of minimizing the free-energy functional (1) which leads to the self-consistent equation

$$\rho(r)=\rho_0 e^{c_0\eta}\exp\left[\sum_{\mathbf{G}(\neq 0)}c(|\mathbf{G}|)\mu_{\mathbf{G}}e^{i\mathbf{G}\cdot\mathbf{r}}\right], \quad (3)$$

where $c(|\mathbf{G}|)$ are the values of (Fourier transform of) the direct correlation function of the liquid (near its freezing point), $c(q)=\rho_0\int d\mathbf{r}\,e^{i\mathbf{q}\cdot\mathbf{r}}c(r)$ at $\mathbf{q}=\mathbf{G}$. $c_0\equiv c(q=0)$ is related to the isothermal compressibility χ_T of the liquid through $\chi_T^{-1}=\rho_0 k_B T(1-c_0)$, and T is the temperature of the liquid.

Equation (3) is equivalent to an infinite set of equations for the order parameters $\mu_{\mathbf{G}}$. In practice, it is not easy to

find solutions to this infinite set of equations, hence, one uses various approximations. One approximation[7,8] that is reasonable is to keep only a finite number of Fourier components because the direct correlation function decreases rapidly at large wave vectors. Over the past few years, many workers[10–13] have used another simple variational choice for the local density of a crystalline solid, namely, a sum of Gaussian density distribution functions centered at the sites of the crystal lattice under consideration. For cubic crystals

$$\frac{\rho(\mathbf{r})}{\rho_0} = A_0 v_{\text{cell}} (\alpha_0/\pi a^2)^{3/2} \sum_{\mathbf{R}} e^{-(\alpha_0/a^2)(\mathbf{R}-\mathbf{r})^2}, \tag{4}$$

where A_0 is the amplitude of the Gaussians, α_0 is their width parameter, a is the cell parameter, v_{cell} is the cell volume ($=a^3/\sqrt{2}$, for fcc crystals), and $\mathbf{R}$ are the direct-lattice vectors of the required lattice.[14] Now, instead of minimizing the free-energy functional (1) with respect to an arbitrary $\rho(\mathbf{r})$, which leads to (3) as a variational approximation, we minimize with respect to functions of the type given by Eq. (4). This is a three-parameter (A_0, α_0, and a) minimization problem. In noncubic crystals, the Gaussian distribution functions will have to be chosen to be anisotropic, implying more parameters.

From Eq. (4), we note that $A_0\rho_0$ gives the number density of the solid (of course, we must use the self-consistently determined parameters A_0, a, and α_0). For a defect-free solid, the solid density is determined by the lattice parameter a alone. Therefore, the value of A_0 contains information about the vacancy concentration in the solid. Since defect densities in a solid are quite low[15] ($\approx 0.2\%$ at the melting point), as a further simplifying approximation we set $A_0=(\rho_0 v_{\text{cell}})^{-1}$, i.e., each of the Gaussian distribution functions in the density function $\rho(\mathbf{r})$ [Eq. (4)] is normalized to unity. Thus, we use

$$\rho(\mathbf{r}) = (\alpha_0/\pi a^2)^{3/2} \sum_{\mathbf{R}} e^{-\alpha_0(\mathbf{R}-\mathbf{r})^2/a^2}. \tag{5}$$

For this form for $\rho(\mathbf{r})$, and neglecting overlaps between Gaussians at different sites, the free-energy functional (1) is given by

$$\frac{\beta F}{N} = \left[\ln\left[\frac{1}{\rho_0} (\beta_0/\pi)^{3/2} \right] - \frac{5}{2} + \rho_0 v_{\text{cell}} \right] - \frac{1}{2\rho_0 v_{\text{cell}}} \sum_{\mathbf{G}} e^{-G^2/2\beta_0} c(G) + c_0 - \tfrac{1}{2}\rho_0 c_0 v_{\text{cell}}, \tag{6}$$

where $\beta_0=\alpha_0/a^2$ and N is the number of lattice sites in the crystal. The term within large square brackets of Eq. (6), is the entropic[16] part of the free-energy functional. Equation (6) is easily minimized to obtain a, α_0, and other freezing parameters in a variety of contexts.

B. Lattice vibrations using the Gaussian density distribution

The density-functional theory can be used to calculate the free energy not only for the equilibrium crystalline state, but also for the uniformly strained crystal (determining the elastic constants)[17] and for more general distortions, e.g., the small atomic displacements involved in lattice vibrations. In this paper we calculate this last mentioned free energy using the simple Gaussian form for the local density.[18]

For this purpose we represent the instantaneous local density in a distorted crystal as a sum of Gaussians centered at $\mathbf{R}+\mathbf{u}(\mathbf{R})$, where the displacements $\mathbf{u}(\mathbf{R})$ are small (so that eventually we can neglect terms of order higher than $|\mathbf{u}(\mathbf{R})|^2$). Since the displacements $\mathbf{u}(\mathbf{R})$ are otherwise arbitrary, each atom of the perturbed solid will be in a different environment (of surrounding atoms). Thus, the Gaussian density distribution about each site will be different and no longer isotropic. Therefore, in general, α_0 will be replaced by $\alpha_0[1+\alpha(\mathbf{R})]$, where $\alpha(\mathbf{R})$ is a symmetric 3×3 matrix. For small $\mathbf{u}$, the elements $\alpha_{ij}(\mathbf{R})$ of $\alpha(\mathbf{R})$ are $O(|\mathbf{u}|)$.[19] We assume that the $\alpha(\mathbf{R})$'s adiabatically follow the instantaneous displacements $\mathbf{u}(\mathbf{R})$ and their dependence on $\mathbf{u}(\mathbf{R})$ is obtained by minimizing the free-energy functional of the distorted solid. The minimized free energy expanded to quadratic order in $\mathbf{u}(\mathbf{R})$ determine the phonon spectra.

For clarity of presentation we give the details of the derivation of phonon dispersion in two steps: (1) We first treat the case when the Gaussian density distribution at any site remains undistorted. (2) Then we include the effects of such distortions.

1. *Phonon dispersion without distortions of Gaussian density distributions*

We consider the change in the free energy ΔF as a result of displacements $\mathbf{u}(\mathbf{R})$ of atoms from their undistorted lattice positions $\mathbf{R}$, determined by the cell parameter a [cf., Eq. (5)]. In calculating ΔF up to terms of $O(u^2)$, in this subsection we assume that, as a result of the displacements $\mathbf{u}(\mathbf{R})$, the Gaussian density distribution at any site is not distorted, and further that these density distributions do not overlap. The details of this calculation are given in Appendix A, and we obtain ΔF as

$$\beta\Delta F = \tfrac{1}{2} \sum_{\mathbf{R}} \sum_{\mathbf{R}'} \sum_{i} \sum_{j} u_i(\mathbf{R}') u_j(\mathbf{R}+\mathbf{R}') \times \left[\sum_{\mathbf{R}_1} \frac{\partial^2 f(\mathbf{R}_1)}{\partial R_{1i}\, \partial R_{1j}} \delta_{R,0} - \frac{\partial^2 f(\mathbf{R})}{\partial R_i\, \partial R_j} \right], \tag{7}$$

$$f(\mathbf{R}) \equiv f(\beta_0, \mathbf{R}) = (\beta_0/2\pi)^{3/2} \int d\mathbf{r}\, c(\mathbf{r}) e^{-\beta_0(\mathbf{R}-\mathbf{r})^2/2}, \tag{8}$$

where $\beta_0=\alpha_0/a^2$ and i and j denote Cartesian components. In Eq. (7) and hereafter the derivatives with respect to R_i are evaluated by assuming R_i to be independent continuous variables. [This is done in order to write the expressions compactly. The actual expression is evaluated in reciprocal space (Appendix A).]

In general, the free-energy change ΔF has two parts:

(1) the entropic part[16] and (2) the interaction part. However, if the Gaussian density distributions are left undistorted, the resulting change in the free-energy functional, given by (7), has no contribution from the entropic part (Appendix A). This is understandable because we have chosen a very simple local density for the solid: nonoverlapping Gaussian density distributions centered at lattice sites $\mathbf{R}$. This amounts to saying that each atom is fixed inside a "shell" centered at $\mathbf{R}$. The change in the free energy is because of change in the positions of these shells from $\mathbf{R}$ to $\mathbf{R}+\mathbf{u}(\mathbf{R})$, without changing anything inside the shells. Therefore, the entropy does not change as a result of the displacements $\mathbf{u}(\mathbf{R})$, and the change in the free energy arises entirely because of the interaction between shells as a result of their relative displacements.

The free-energy change (7) has the same form as it does in the case of the Born–von Kármán force-constant model, but the interpretation of the terms involved is different. Since the widths of the Gaussian density distributions are very narrow (we show in Sec. IV that $\alpha_0 > 100$), from Eqs. (7) and (8) it follows that

$$f(\mathbf{R}) \approx c(R)$$

and (9)

$$\frac{\partial^2 f(\mathbf{R})}{\partial R_i \, \partial R_j} \approx \frac{\partial^2 c(R)}{\partial R_i \, \partial R_j}$$

for all $\mathbf{R}$. Therefore, to the leading order in $1/\alpha_0$, the interatomic potential in the quasiharmonic force constant model of Born and von Kármán is replaced by $k_B T$ times the direct correlation function $c(r)$ of the liquid at its freezing point (or better, the supercooled liquid). It is important to note that the range of the direct correlation function, at least for simple systems, is small [appreciable only up to fourth-nearest atomic shells (Sec. IV D)]. $c(r)$ can be calculated from the experimentally measured structure factor $S(q)$ of liquid, through its Fourier transform $c(q)$: $c(q)=1-1/S(q)$.

An approximation in which the Gaussian density distribution about a site is not allowed to deform (relax), will yield higher phonon frequencies than a treatment in which this deformation is allowed, since, in the former case, the crystal is stiffer than in the latter. We now describe a calculation of phonon frequencies which allows for such deformation.

2. *Phonon dispersion with distortions of Gaussian density distribution*

As discussed earlier the deformation of the Gaussian density distribution as the atoms are displaced from $\mathbf{R}$ is described by a change in the width parameter α_0, to a symmetric matrix $\alpha_0[\mathbf{1}+\boldsymbol{\alpha}(\mathbf{R})]$ that depends on $\mathbf{R}$. We have also mentioned earlier[19] that $|\alpha_{ij}(\mathbf{R})| \approx |\mathbf{u}(\mathbf{R})|$. We calculate the change in the free energy of the solid because of these displacements under the assumption that the Gaussian density distributions at different sites do not overlap. The calculation is done in two steps: (1) First we take the $\alpha_{ij}(\mathbf{R})$ to be arbitrary and calculate the change in free energy. (2) Next we select those $\alpha_{ij}(\mathbf{R})$ which minimize the free energy for the set of displacements $\mathbf{u}(\mathbf{R})$. Thus, we express $\alpha_{ij}(\mathbf{R})$ as functions of the displacements $\mathbf{u}(\mathbf{R})$. This leads to a modification of the force constants calculated in the previous subsection B(1) and hence to a modification of the phonon frequencies.

The free-energy change ΔF in the presence of distortions of the Gaussian density distributions centered at $\{\mathbf{R}+\mathbf{u}(\mathbf{R})\}$ is given by (see Appendix B for details)

$$\beta \Delta F = \tfrac{1}{2} \sum_{\mathbf{R}} \sum_{\mathbf{R}'} \left[\sum_{i,j} u_i(\mathbf{R}') H_1^{ij}(\mathbf{R}) u_j(\mathbf{R}+\mathbf{R}') + \sum_{i,j,k} u_i(\mathbf{R}') H_2^{ijk}(\mathbf{R}) \alpha_{jk}(\mathbf{R}+\mathbf{R}') + \sum_{i,j,k} \alpha_{ij}(\mathbf{R}') H_3^{ijk}(\mathbf{R}) u_k(\mathbf{R}+\mathbf{R}') + \sum_{\substack{i,j \\ k,m}} \alpha_{ij}(\mathbf{R}') H_4^{ijkm}(\mathbf{R}) \alpha_{km}(\mathbf{R}+\mathbf{R}') \right] . \tag{10}$$

Here,

$$H_1^{ij}(\mathbf{R}) = -\sum_{\mathbf{R}_1} \frac{\partial^2 f(\mathbf{R}_1)}{\partial R_{1i} \partial R_{1j}} \delta_{\mathbf{R},0} + \frac{\partial^2 f(\mathbf{R})}{\partial R_i \partial R_j} , \tag{11a}$$

$$H_2^{ijk}(\mathbf{R}) = -(1/4\beta_0) \left[\frac{\partial^3 f(\mathbf{R})}{\partial R_i \partial R_j \partial R_k} + \sum_{\mathbf{R}_1} \frac{\partial^3 f(\mathbf{R}_1)}{\partial R_{1i} \partial R_{1j} \partial R_{1k}} \delta_{R,0} \right] , \tag{11b}$$

$$H_3^{ijk}(\mathbf{R}) = (1/4\beta_0) \left[\frac{\partial^3 f(\mathbf{R})}{\partial R_i \partial R_j \partial R_k} - \sum_{\mathbf{R}_1} \frac{\partial^3 f(\mathbf{R}_1)}{\partial R_{1i} \partial R_{1j} \partial R_{1k}} \delta_{R,0} \right] , \tag{11c}$$

$$H_4^{ijk}(\mathbf{R}) = X + Y , \tag{11d}$$

where

$$X \equiv -\delta_{R,0}[\tfrac{1}{4}(\delta_{im}\delta_{jk}+\delta_{ik}\delta_{jm}) , \tag{12}$$

$$Y \equiv -\delta_{R,0}\left[\frac{1}{16\beta_0^2}\sum_{\mathbf{R}_1}\frac{\partial^4 f(\mathbf{R}_1)}{\partial R_{1i1j}\,\partial R_{1k}\,\partial R_{1m}} + \frac{1}{8\beta_0}\sum_{\mathbf{R}_1}\left[\frac{\partial^2 f(\mathbf{R}_1)}{\partial R_{1j}\,\partial R_{1m}}\delta_{ik}+\frac{\partial^2 f(\mathbf{R}_1)}{\partial R_{1j}\,\partial R_{1k}}\delta_{im}+\frac{\partial^2 f(\mathbf{R}_1)}{\partial R_{1i}\partial R_{1m}}\delta_{jk}+\frac{\partial^2 f(\mathbf{R}_1)}{\partial R_{1i}\,\partial R_{1k}}\delta_{jm}\right]\right] - \frac{1}{16\beta_0^2}\frac{\partial^4 f(\mathbf{R})}{\partial R_i\,\partial R_j\,\partial R_k\,\partial R_m} . \tag{13}$$

Here $f(\mathbf{R})$ is same as defined in Eq. (8). Only the part X [cf., Eqs. 11(d) and 12] of the last term of Eq. (10) determines the entropic contribution[16] to the free-energy change (Appendix B) and is thus given by

$$\beta\Delta F_{\text{ent}} = \tfrac{1}{2}\sum_{\mathbf{R}}\sum_{i,j=1}^{3}\tfrac{1}{2}[\alpha_{ij}(\mathbf{R})]^2 . \tag{14}$$

It is clear that this contribution arises because of the deformation of the Gaussian density distributions alone and it is a sum of the contributions from each "shell" (see Sec. II B 1). Since $\alpha(\mathbf{R})$ is a symmetric, 3×3 matrix, it has only six independent components. We relabel these as $\phi_\mu(\mathbf{R})\equiv K_{ij}\alpha_{ij}(\mathbf{R})$ with K_{ij} a numerical factor, and similarly define $F_1^{ij}\equiv H_1^{ij}$, $F_2^{i\mu}\equiv H_2^{ijk}$, $F_3^{\mu k}\equiv H_3^{ijk}$, $F_4^{\mu\sigma}\equiv H_4^{ijkm}$, where Greek indices (for example, μ) are related to pairs of Latin indices (for example, ij) as shown in Table I. Then we can write

$$\beta\Delta F = \tfrac{1}{2}\sum_{\mathbf{R}}\sum_{\mathbf{R}'}\left[\sum_{i,j=1}^{3}u_i(\mathbf{R}')F_1^{ij}(\mathbf{R})u_j(\mathbf{R}+\mathbf{R}')+\sum_{i=1}^{3}\sum_{\mu=1}^{6}u_i(\mathbf{R}')F_2^{i\mu}(\mathbf{R})\phi_\mu(\mathbf{R}+\mathbf{R}') + \sum_{i=1}^{3}\sum_{\mu=1}^{6}\phi_\mu(\mathbf{R}')F_3^{\mu i}(\mathbf{R})u_i(\mathbf{R}+\mathbf{R}')+\sum_{\mu=1}^{6}\sum_{\nu=1}^{6}\phi_\mu(\mathbf{R}')F_4^{\mu\nu}(\mathbf{R})\phi_\nu(\mathbf{R}+\mathbf{R}')\right] . \tag{15}$$

The terms in Eq. (15) have analogues in the phenomenological lattice-dynamical theory of ionic solids.[20,21] The variables ϕ are the analogues of the dipole moments, the coefficients F_2 and F_3 of the effective charge tensor, and the coefficients F_4 of the electronic polarizability tensor of the (ionic solid) medium. The ions are deformed because of the overlapping of the electronic charge clouds of neighboring ions. The analogy is not exact because, in the case of ionic solids, the dipolar fields extend to large distances, whereas the effective interaction in our density-functional theory is given by the direct correlation function which is short ranged (Sec. IV D). Further, in an ionic solid, the deformation is because of the physical overlapping of the electron clouds, whereas in our theory the deformation arises because of a change in the statistical distribution of the centers of atoms (as a result of the change in the relative positions of atoms).

We now minimize Eq. (15) with respect to the $\phi_\mu(\mathbf{R})$'s keeping $\mathbf{u}(\mathbf{R})$ fixed. As a result of this minimization, the set $\phi_\mu(\mathbf{R})$'s are now expressed in terms of the displacements $\mathbf{u}(\mathbf{R})$. This is conveniently carried out in the momentum space (Appendix C). The Fourier components

$$\phi_\mu(\mathbf{q}) = \sum_{\mathbf{R}}\phi_\mu(\mathbf{R})e^{i\mathbf{q}\cdot\mathbf{R}}$$

are given by

$$\phi_\mu(\mathbf{q}) = -\sum_{i=1}^{3}\sum_{\sigma=1}^{6}u_i(\mathbf{q})E_2^{i\sigma}(\mathbf{q})[E_4^{-1}(\mathbf{q})]^{\sigma\mu} = -\sum_{\sigma=1}^{6}\sum_{i=1}^{3}[E_4^{-1}(\mathbf{q})]^{\mu\sigma}E_3^{\sigma i}(-\mathbf{q})u_i(\mathbf{q}) , \tag{16}$$

where

$$E_m(\mathbf{q}) = \sum_{\mathbf{R}}e^{i\mathbf{q}\cdot\mathbf{R}}F_m(\mathbf{R}), \quad m=1,2,3,4 .$$

At the minimum, the free-energy change ΔF is of the conventional form

$$\beta\Delta F = \tfrac{1}{2}\sum_{\mathbf{q}}\sum_{i,j=1}^{3}u_i(\mathbf{q})D^{ij}(\mathbf{q})u_j(-\mathbf{q}) \tag{17}$$

TABLE I. The pair of indices (i,j) in each column of the first row are replaced by the index (μ) of the same column of the second row. $\phi_\mu(\mathbf{R})$ are defined as $K_{ij}\alpha_{ij}(\mathbf{R})$. The factors K_{ij} are given in the third row.

$(i,j)\rightarrow$	1,1	1,2 (2,1)	1,3 (3,1)	2,2	2,3 (3,2)	3,3
$\mu\rightarrow$	1	2	3	4	5	6
$K_{ij}\rightarrow$	1	2	2	1	2	1

with the effective dynamical matrix (Fourier transform of the force constants) $D(\mathbf{q})$ being given by

$$\beta D^{ij}(\mathbf{q})=E_1^{ij}(\mathbf{q})-\sum_{\mu,\sigma=1}^{6} E_2^{i\mu}(\mathbf{q})[E_4^{-1}(\mathbf{q})]^{\mu\sigma}E_3^{\sigma j}(\mathbf{q}) . \tag{18}$$

If we define

$$\begin{aligned}
&\varepsilon_1^{ij}(\mathbf{q})=E_1^{ij}(\mathbf{q}) ,\\
&\varepsilon_2^{ijk}(\mathbf{q})=E_2^{i\mu}(\mathbf{q}) ,\\
&\varepsilon_3^{ijk}(\mathbf{q})=E_3^{\mu k}(\mathbf{q}) ,\\
&\varepsilon_4^{ijkm}(\mathbf{q})=E_4^{\mu\sigma}(\mathbf{q}) ,
\end{aligned} \tag{19}$$

then [by Fourier transforming H_m's of Eqs. (11)], we get

$$\varepsilon_1^{ij}(\mathbf{q})=\frac{1}{\rho_0 v_{\text{cell}}}\left[\sum_G e^{-G^2/2\beta_0}c(G)G_iG_j-\sum_{\mathbf{G}} e^{-(\mathbf{G}+\mathbf{q})^2/2\beta_0}c(|\mathbf{G}+\mathbf{q}|)\times(\mathbf{G}+\mathbf{q})_i(\mathbf{G}+\mathbf{q})_j\right] , \tag{20a}$$

$$\varepsilon_2^{ijk}(\mathbf{q})=\frac{\sqrt{-1}}{4\beta_0\rho_0 v_{\text{cell}}}\sum_{\mathbf{G}} e^{-(\mathbf{G}+\mathbf{q})^2/2\beta_0}c(|\mathbf{G}+\mathbf{q}|)\times(\mathbf{G}+\mathbf{q})_i(\mathbf{G}+\mathbf{q})_j(\mathbf{G}+\mathbf{q})_k=-\varepsilon_3^{ijk}(\mathbf{q}) , \tag{20b}$$

and

$$\varepsilon_4^{ijkm}(\mathbf{q})=-\tfrac{1}{4}(\delta_{im}\delta_{jk}+\delta_{ik}\delta_{jm})+\frac{1}{16\beta_0\rho_0 v_{\text{cell}}}\left[\sum_{\mathbf{G}} e^{-G^2/2\beta_0}c(G)[-G_iG_jG_kG_m/\beta_0+2(\delta_{ik}G_jG_m+\delta_{im}G_jG_k+\delta_{jk}G_iG_m+\delta_{jm}G_iG_k)]-\beta_0^{-1}\sum_{\mathbf{G}} e^{-(\mathbf{G}+\mathbf{q})^2/2\beta_0}c(|\mathbf{G}+\mathbf{q}|)(\mathbf{G}+\mathbf{q})_i(\mathbf{G}+\mathbf{q})_j(\mathbf{G}+\mathbf{q})_k(\mathbf{G}+\mathbf{q})_m\right] , \tag{20c}$$

where, as defined earlier, $\beta_0=\alpha_0/a^2$ and v_{cell} is the primitive-cell volume ($=a^3/\sqrt{2}$ for the fcc crystal).

It is clear from Eq. (18) that the dynamical matrix consists of two parts: (1) $\mathbf{E}_1(\mathbf{q})$, which comes solely from the displacements $\mathbf{u}(\mathbf{R})$, and (2) $-\mathbf{E}_2(\mathbf{q})[\mathbf{E}_4^{-1}(\mathbf{q})]\mathbf{E}_3(\mathbf{q})$, which arises because of the distortion of the Gaussian density distributions at sites. It can be seen easily that $\mathbf{E}_1(\mathbf{q})$, $\mathbf{E}_2(\mathbf{q})$, and $\mathbf{E}_3(\mathbf{q})$ go to zero as $\mathbf{q}$ goes to zero [from Eqs. (19) and (20)] and therefore we obtain only acoustic modes of vibration as expected of a crystal with a single atom per unit cell. Also, note that $\boldsymbol{\varepsilon}_1(\mathbf{q})$ becomes zero only at $\mathbf{q}=n\mathbf{G}$ [Eq. (20a)], where $\mathbf{G}$ is any reciprocal-lattice vector and n is any integer, but $\boldsymbol{\varepsilon}_2(\mathbf{q})$ and $\boldsymbol{\varepsilon}_3(\mathbf{q})$ [Eq. (20b)] become zero at $\mathbf{q}=(n/2)\mathbf{G}$. Thus, the frequencies of vibration at the zone boundaries are unaffected by the deformation of the Gaussian density distribution.

The elastic constants of the crystal at its melting point can be calculated in the standard way from the dynamical matrix (18). The calculation is given in Appendix D and its results are discussed in Sec. IV.

III. STRUCTURE FACTORS USED IN OUR CALCULATIONS

The input required for our theory (Sec. II) is the direct correlation function $c(r)$ of the liquid (say, argon) just above its freezing point (or better, of supercooled liquid argon). $c(r)$ is related to the structure factor $S(q)$ of the liquid through the relation $S(q)=[1-c(q)]^{-1}$, where $c(q)=\rho_0\int d\mathbf{r}\, c(r)e^{i\mathbf{q}\cdot\mathbf{r}}$, and ρ_0 is the number density of the liquid. The structure factor $S(q)$ of the liquid is either measured experimentally or calculated from approximate theories of liquids. In the following, we describe the structure factors we use to calculate the phonon dispersion in and elastic constants of crystalline argon near its melting point. We also discuss the shortcomings of various available structure factors. We then present our numerical results in Sec. IV.

Typically in experiments the structure factor $S(q)$ of a liquid is measured along the liquid-vapor saturation line which meets the liquid solid phase boundary at the triple point where solid, liquid, and vapor coexist. The triple point of argon is at 83.81 K and 0.68 atmosphere of pressure.[22] There are some measurements of $S(q)$ of liquid argon close to the triple point, namely, those of (1) Page[23] at 84.5 K and (2) Yarnell *et al.*[24] at 85 K. Apart from these experimentally measured structure factors, we also use a numerically calculated $S(q)$ for a Lennard-Jones fluid with parameters appropriate for a description of liquid argon.

A. Structure factors from experiments

First we describe Yarnell *et al.*'s[24] data. They measure the structure factor $S(q)$ of liquid argon in equilibrium with its vapor at 85 K and at an atomic density of 0.021 25 Å^{-3} by neutron scattering. They measure $S(q)$ up to $q\approx 9$ Å^{-1} [far enough to obtain four peaks of $S(q)$]. They estimate that the overall systematic error in the refined experimental values of $S(q)$ is less than 0.01 for all values of q. Yarnell *et al.* do not present their ac-

tual (refined) experimental data in the paper.[24] The experimental data are extended to high-q values (up to $q \approx 11.75$ Å^{-1}) and also to low-q values ($q=0$ included). They use the results of a molecular-dynamic calculation[25] as a guide for extending the experimental data to large q. The low-q data are extended smoothly to the compressibility limit at $q=0$. [Isothermal compressibility $=2.12\times10^{-4}$ atm,[22] which is equivalent to $S(q=0)=0.0524$.] The extended data are then subjected to an iterative procedure suggested by Verlet for smoothing: The data for $S(q)$ are Fourier transformed to get the radial distribution function $g(r)$. The radial distribution is then modified so that $g(r)=0$ for r up to 0.8 atomic diameter (because the hard-core repulsion prevents atomic overlap). Then the unreasonable humps and dips of $g(r)$ are smoothed out (because oscillations of wavelengths small compared to the atomic diameter are not expected). This modified $g(r)$ is then transformed back to $S(q)$. The resulting $S(q)$ is then smoothed to suppress any remaining short-wavelength oscillations. This procedure is iterated until the extended and smoothed data for $S(q)$ agree with the experimental data for $S(q)$ over the entire available range of q.

We use these extended data (henceforth called Yarnell's data) in our calculation. Although Yarnell's data are smooth, they are not smooth enough to get reasonable derivatives. (For some parts of our calculation we need first and second derivatives.) The data still have some high-frequency noise. We generate a new set of data at uniform intervals of 0.01 Å^{-1} using a cubic-spline interpolation scheme for Yarnell's data. The interpolated data are then smoothed in the following manner: The first peak is carefully fit by an exponential function. The part of $S(q)$ from $q=0$ to the first peak is fit in several parts by a polynomial fit.[26] From the first peak to $q=5.5$ Å^{-1} are fit the data for $S(q)$ in several parts using a polynomial fit. We fit the rest of the high-q part of the interpolated $S(q)$ data by filtering to get rid of high-frequency noise using a fast-Fourier transform program. Since it is very difficult to remove discontinuities at the meeting points of these parts of the fits to the $S(q)$ data, we choose the meeting points in such a way that, in our calculation, we do not need the data (particularly the derivatives) at those points (i.e., care is taken so that the reciprocal-lattice vectors we use do not fall near the joining points). Our fit for $S(q)$ agrees well with Yarnell's data; the differences are never more than 0.7% from the first peak (at q_0) to the largest-q value in Yarnell's data, and never more than 2% for $0<q<q_0$ [a region of $S(q)$ curve that does not affect our results significantly]. We took special care to ensure that, at the first peak, the deviation was never more than 0.3% (this is done because the first peak is very sharply peaked). We use this fit in our calculations.

The second set of experimental, neutron-scattering data for $S(q)$ of liquid argon in equilibrium with its vapor is by Page.[23] These data are at a temperature of 84.5 K and an atomic density of 0.021 29 Å^{-3} (obtained by linear interpolation from the data given by Hunter and Rowlinson[22]). The experimental data range from $q=0.7$ to 8.1 Å^{-1} at intervals of 0.1 Å^{-1}. The structure factor data

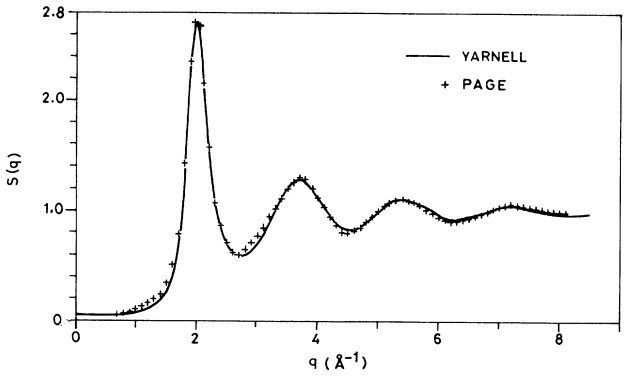

FIG. 2. Structure-factor data for liquid argon near its freezing point along the liquid-gas phase boundary: (a) At 85 K (solid line), as measured by Yarnell *et al.* (Ref. 24), (b) at 84.5 K (crosses), as measured by Page (Ref. 23).

are given to two decimal places. Page's data compare very well with Yarnell's data except in the low-q region. Yarnell's data and Page's data are plotted together for comparison in Fig. 2. Since the data stop at $q=0.7$ Å^{-1} on the low-q side and the measurements are not very accurate in that region, we replace Page's data on the left side of the first peak by Yarnell's data in that region. Since the data points are not closely spaced and are not smooth (i.e., have some high-frequency noise), we obtained a fit to the data. We did this by using an exponential function at the first peak and polynomials for the rest of the data range. Since we fit the $S(q)$ data by smooth functions, the derivatives are continuous at all points except at the points where fits to different regions of the data are joined to cover the complete range of $S(q)$. We use two fits: (1) One in which the data are roughly such that the positions of the meeting points of different fitted pieces were taken conveniently; the fit data (called P_1) never differs from the experimental data by more than 2% (except at two points where the error is about 3%). (2) The second fit (called P_2) is such that the meeting points do not fall close to the reciprocal-lattice vectors we use; this fit never differs from the first fit P_1 or the experimental data by more than 2% (except at the same points where the first fit P_1 differs from the experimental data by about 3%).

B. Numerically calculated $S(q)$

There are many numerical simulation (say, molecular-dynamic) studies of the radial distribution function $g(r)$ of Lennard-Jones (LJ) systems (in which particles interact via a pair potential $v(r)=4\varepsilon[(\sigma/r)^6-(\sigma/r)^{12}]$) at various temperatures and densities. Goldman[27] has proposed an empirical formula to represent these numerical simulation results for $g(r)$ as a function of density and temperature. The empirical formula covers the following ranges of temperature T and density ρ_0: $0.5\varepsilon/k_B \le T < 5.0\varepsilon/k_B$, and $0.35\sigma^{-3} \le \rho_0 < 1.10\sigma^{-3}$. Goldman's formula was proposed originally to fit the

molecular-dynamic data up to a distance of $r \approx 4.5\sigma$. We chose the Lennard-Jones parameters $\sigma = 3.405$ Å and $\varepsilon/k_B = 119.8$ K for liquid argon (following Verlet's fit to Levelt's[28] thermodynamic data). Since $g(r)$ does not differ much from 1 at distance larger than 4.5σ, and since Goldman's formula also gives $g(r)$ close to 1 at these distances, we assume this formula to be valid up to 50σ. We use the $g(r)$ thus obtained to calculate the structure factor $S(q)$ by using the relation

$$S(q) = 1 + \rho_0 \int d\mathbf{r}\, e^{i\mathbf{q}\cdot\mathbf{r}} [g(r) - 1] \, .$$

We have to extend the data for $g(r)$ up to a large distance 50σ to find $S(q)$ (using a numerical Fourier transform) at finely spaced values of q. Such a fine spacing is essential at the first peak of $S(q)$, since it is very sharp.

The structure factor that we obtained from our extension of Goldman's data for $g(r)$ (as described above) suffers from one problem: At low values of q [between $q = 0$ and the highest maximum of $S(q)$], this structure factor oscillates about zero and remains negative (≈ -0.25) at $q = 0$. This is clearly an unphysical behavior, for it leads to a negative compressibility. (Similar problems with Goldman's fit have been reported by Marshall, Laird, and Haymet.[29]) To rid our $S(q)$ of this unphysical behavior, we proceed as follows: We fix the value of $S(q = 0)$ by using the 33-parameter empirical fit of Nicolas *et al.*,[30] to the compressibility of a Lennard-Jones fluid as a function of T and ρ_0. We then scale Yarnell's data for argon (see above) to join smoothly $S(q = 0)$ (from Nicolas *et al.*) to the highest peak of $S(q)$ (obtained from our extension of Goldman's fit). The sharp first peak of $S(q)$ is fit carefully using an exponential function. The structure factor obtained as a Fourier transform of $g(r)$ is plotted in Fig. 3 along with its (just described) modified version which we will use in our calculations.

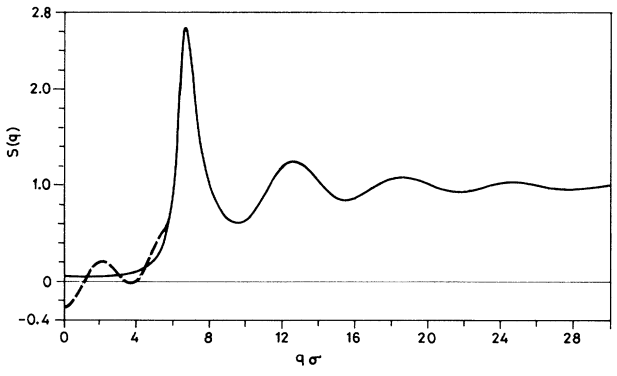

FIG. 3. The structure factor $S(q)$ of a Lennard-Jones fluid obtained from Goldman's fit (dashed line) to the numerically obtained results for the radial distribution function (at the reduced temperature, $T^* = 0.9$, and the reduced density, $\rho^* = 0.8233$). The solid line shows the structure factor that is obtained from our modification of Goldman's fit (see text). Our modification and Goldman's fit lead to significant differences in $S(q)$ only at small values of q.

IV. NUMERICAL RESULTS

A. Freezing of liquid argon

Before calculating the phonon dispersion of crystalline argon at its melting temperature, we need the cell parameter a and the Gaussian-width parameter α_0 of the local density $\rho(\mathbf{r})$ [Eq. (5)] describing the solid when it freezes. These parameters depend on the structure factor $S(q)$ of the liquid just above its freezing point. As mentioned earlier (Sec. III), we use three sets of data for the structure factor of liquid argon. For all the three structure factors we follow the same procedure to find a and α_0 so as to minimize the free-energy functional [Eq. (6)] and use these values for a and α_0 in our calculation of phonon dispersion.

As is mentioned in Sec. III A, Yarnell's data for $S(q)$ extends to a fairly large value of q (≈ 11.75 Å^{-1}). To check whether the range of data available is sufficient for our calculation, we evaluate the minimum of the free-energy functional [Eq. (6)] by using various values of N_s, the number of reciprocal-lattice vector shells in the summation in Eq. (6). Figure 4(a) shows how the value of the free-energy functional at its minimum changes with N_s. In Figs. 4(b) and 4(c) we plot, respectively, a and α_0 at this minimum versus N_s. As is clear from Figs. 4(b) and 4(c), the variation of the cell parameter a with N_s is small, but α_0 varies appreciably with N_s, though after $N_s = 41$, this variation is small. This indicates that, ideally, we should go beyond $N_s = 44$; unfortunately, this would entail going beyond the range of Yarnell's data. Most of our calculations are done with two values of N_s: $N_s = 39$ and 44. For comparison the free-energy functionals and α_0's (for $N_s = 39$ and 44) versus a are plotted, respectively, in Figs. 5(a) and 5(b).

If we use $N_s = 39$, we get $a = 3.771$ Å, $\alpha_0 = 526.16$, and a free energy (F) of $-0.1237 k_B T$ ($T = 85$ K). For $N_s = 44$, we get $a = 3.776$ Å, $\alpha_0 = 451.41$, and $F = -0.0758 k_B T$. Note that even at a temperature of 85 K, at which argon is a liquid, we get a stable solid (with $N_s = 39$ and 44). We believe that this stability of solid argon at the higher temperature is due to the various approximations in our calculation, including the incomplete-poor structure factor data used (see Sec. V).

Since Page's data for $S(q)$ extend up to $q \approx 8$ Å^{-1}, we are restricted to $N_s \leq 18$, so we use $N_s = 18$. As has been mentioned in Sec. III A, we fit Page's data in two ways denoted by P_1 and P_2 (these fits do not differ from one another by more than 2% anywhere in the data range except at two points). We calculate the free-energy functional using both fits P_1 and P_2. For comparison of results (using fits P_1 and P_2), the free-energy functional (minimized with respect to α_0) and the values of α_0 are plotted versus cell parameter a; they are shown, respectively, in Figs. 6(a) and 6(b). We obtain the following results at the minimum of free-energy functional for the fit P_1, $a = 3.81$ Å, $\alpha_0 = 499.8$, and $F = -0.518 k_B T$ ($T = 84.5$ K); and for the fit P_2, $a = 3.815$ Å, $\alpha_0 = 541.12$, and $F = -0.7764 k_B T$. Note that α_0 (but not a), is very sensitive to the fits: the values of α_0 obtained from these

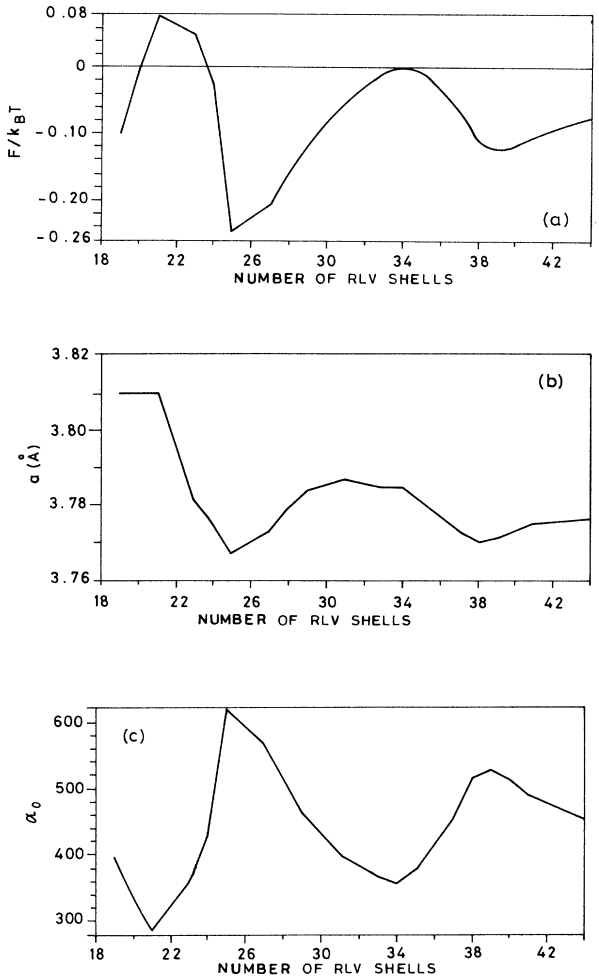

FIG. 4. The variation with N_s (the number of reciprocal-lattice-vector shells used in our calculation) of (a) the value of free-energy functional at its global minimum, (b) the corresponding cell parameter a, and (c) the corresponding width parameter α_0. For this figure we use structure-factor data of Yarnell *et al.* (Ref. 24).

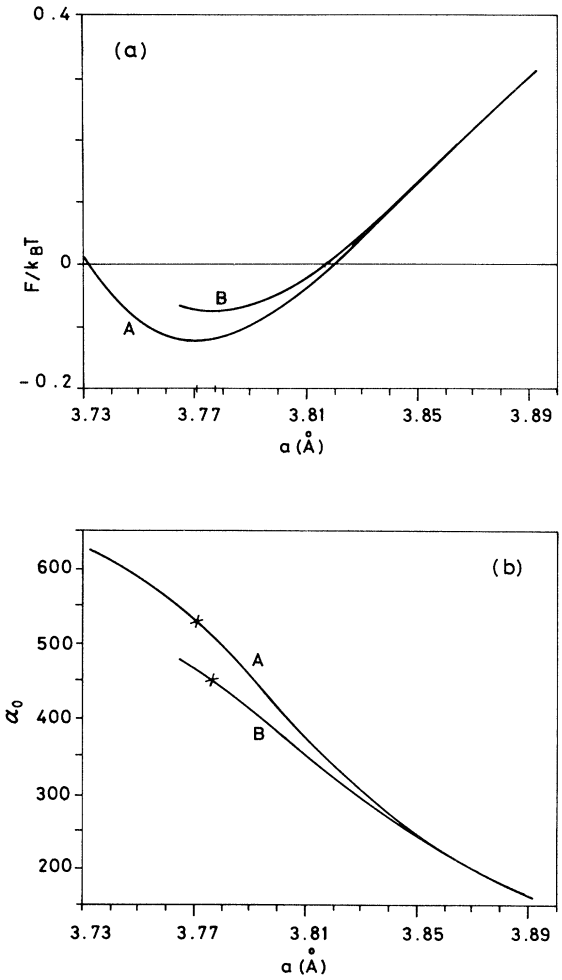

FIG. 5. The variation with the cell parameter a of (a) the value of the free-energy functional (F), minimized with respect to the width parameter α_0, and (b) the width parameter at this minimum (the crosses show the position of global minimum of F). For this figure we use the structure-factor data of Yarnell *et al.* (Ref. 24) and $N_s=39$ (marked A) and $N_s=44$ (marked B).

two fits differ by about 10%. This is because the cell parameter a is fixed, more or less, by the position of the first peak of $S(q)$, whereas small differences in the values of $S(q)$ at large q change the free-energy functional (and, hence, α_0) appreciably because certain reciprocal-lattice vector shells contain large numbers of vectors (up to 48). Therefore, accurate measurements of $S(q)$ and good interpolation schemes are necessary to obtain good results from the density-functional theory.

As mentioned in Sec. III B, we obtain $S(q)$ of liquid argon from numerical simulations of a Lennard-Jones fluid for a large range of densities and temperatures. We can, therefore, use the density-functional theory to find the liquid-solid phase boundary in this range of densities and temperatures. Also, since we can get $S(q)$ up to large values of q, the problem of the dependence of freezing parameters a and α_0 on the number of reciprocal-lattice vector shells N_s used is easily solved. We find that F [Eq. (6)] differ by only about 2% if N_s is changed from 50 to 100. Thus, we use $N_s=50$ in our calculation. With the Lennard-Jones parameters we use to describe liquid argon ($\varepsilon/k_B=119.8$ K and $\sigma=3.405$ Å), the triple point should occur at $T=0.7\varepsilon/k_B$. But we do not find liquid in equilibrium with solid below $T=0.85\varepsilon/k_B$ at any ρ_0. This may be because the structure factor we are using is not as accurate as it should be; moreover, our density-functional neglects higher-order correlation functions and we use an approximation for $\rho(r)$, namely a sum of Gaussian density distributions centered at the lattice sites. In our study, we restrict ourselves to the solid side

of one point ($T=0.9\varepsilon/k_B$ and $\rho_0=0.0208$ Å^{-3}) of the liquid-solid phase boundary. The freezing parameters at this point are $a=3.82$ Å and $\alpha_0=278.9$.

B. Calculation of elastic constants

As is well known, the elastic properties of solid are revealed in the long-wavelength limit of its lattice vibrations. The elastic constants[17] are calculated from the velocities of sound obtained from the phonon dispersion curves in the small-q (wave-vector) limit. The velocities of sound can be measured in either of the two (equivalent) ways: by taking the limiting expression for the eigenvalues of the dynamical matrix, or by measuring the slopes of the calculated phonon dispersion curves at $q=0$. In this section we look at the limiting ($q\rightarrow 0$) expressions for the elements of the dynamical matrix and discuss the velocities of sound we obtain. For simplicity, we focus our attention on the wave propagation in the (200)-symmetry direction of the crystal because, in this direction, the dynamical matrix is diagonal and the expressions become simple. For clarity we discuss the longitudinal and transverse modes of lattice vibrations separately.

1. *Longitudinal mode of vibration*

As we discussed in Sec. II, the dynamical matrix has two parts: (a) the contribution because of the displacements of atoms from their equilibrium positions (we call this the U part), and (b) the contribution because of the distortion of the Gaussian density distributions in our representation for $\rho(\mathbf{r})$ in the solid phase [Eq. (5)] (we call this the ϕ part or, simply, the correction term). The longitudinal velocity of sound v_l in the (200) direction turns out to be (Appendix D) such that

$$M\beta v_l^2 = A_l + B_l \ , \tag{21}$$

where

$$A_l = -\frac{1}{\rho_0 v_{\text{cell}}}\left\{\sum_{\mathbf{G}(\neq 0)} e^{-G^2/2\beta_0}\left[c(G)\left[1-\frac{5}{2}\frac{G_1^2}{\beta_0}\right]+\frac{dc(G)}{dG}\left[-\frac{G_1^4}{\beta_0 G}+\frac{5}{2}\frac{G_1^2}{G}-\frac{1}{2}\frac{G_1^4}{G^3}\right]+\frac{d^2c(G)}{dG^2}\left[\frac{1}{2}\frac{G_1^4}{G^2}\right]\right]+c_0\right\} \tag{22a}$$

is the contribution from the U part and

$$B_l = \frac{1/8\left[(1/(\beta_0\rho_0 v_{\text{cell}}))\sum_{\mathbf{G}} e^{-G^2/2\beta_0}\{c(G)[3G_1^2-G_1^4/\beta_0]+[dc(G)/dG](G_1^4/G)\}\right]^2}{\left[1+(1/\rho_0 v_{\text{cell}})\sum_{\mathbf{G}} e^{-G^2/2\beta_0}c(G)(G_1^2/\beta_0)(\frac{1}{4}G_1^2/\beta_0-1)\right]} \tag{22b}$$

is the contribution from the ϕ part of the dynamical matrix, $\beta_0=a^2/\alpha_0$, G_i is the ith component of the reciprocal-lattice vector $\mathbf{G}$, v_{cell} is the volume of a primitive cell of an argon crystal (fcc), $\beta=(k_BT)^{-1}$, T is the absolute temperature, k_B is the Boltzmann constant, M is the mass of an argon atom, and $c_0=c(q=0)$. Note that the U part, Eq. (22a), has a term $-c_0/(\rho_0 v_{\text{cell}})$. This should be compared with the velocity of sound in liquid v_{liq}, given by $\beta M v_{\text{liq}}^2=(1-c_0)$ (from compressibility data for liquid argon at $T=85$ K, $c_0\approx -18$). The factor ac-

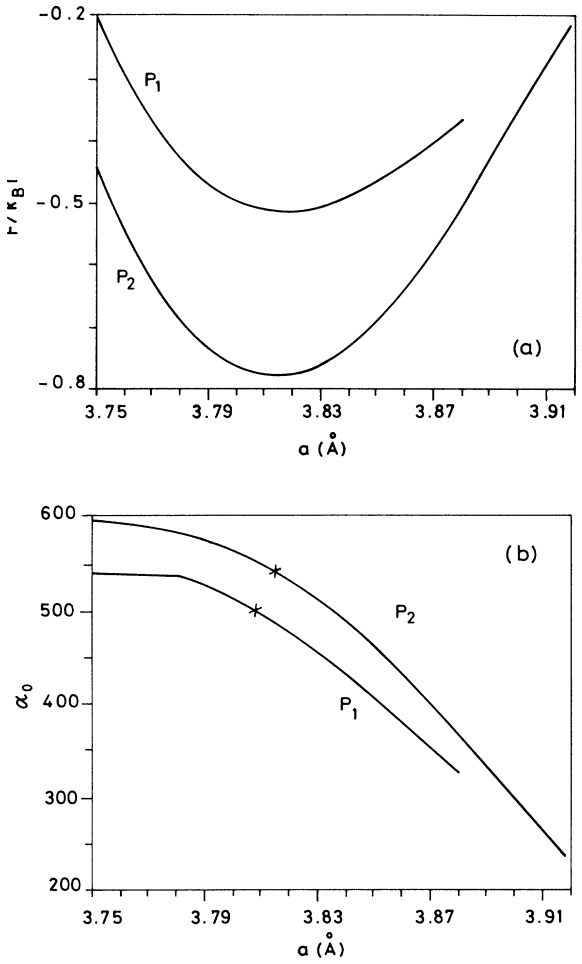

FIG. 6. The same as Fig. 5 but using the fits P_1 and P_2 (see text) to Page's structure-factor data (Ref. 23). In both cases we use $N_s=18$.

companying c_0 is the ratio of the densities of solid and liquid at the freezing point. The rest of the U part, namely, the terms added to $-c_0/(\rho_0 v_{\text{cell}})$, and all of the ϕ part [Eq. (22b)] are a correction to the velocity of sound in the solid, obtained by using liquid-state properties. This correction depends on the structure of the solid, described by the reciprocal-lattice vectors **G**.

2. Transverse modes of vibration

For a wave propagation in the (200) direction, the transverse modes of vibration have identical velocities v_t, which is given by (Appendix D)

$$M\beta v_t^2 = A_t + B_t \ , \tag{23}$$

where

$$A_t = -\frac{1}{\rho_0 v_{\text{cell}}} \sum_{\mathbf{G}} e^{-G^2/\beta_0} \left[c(G) \left[-1/2 \frac{G_2^2}{\beta_0} \right] + \frac{dc(G)}{dG} \left[-\frac{G_2^2 G_3^2}{\beta_0 G} + \frac{G_2^2}{2G} - 1/2 \frac{G_2^2 G_3^2}{G^3} \right] + \frac{d^2 c(G)}{dG^2} \left[1/2 \frac{G_2^2 G_3^2}{G^2} \right] \right] \tag{24a}$$

is the contribution from the U part of the dynamical matrix and

$$B_t = \frac{\left[(1/\beta_0 \rho_0 v_{\text{cell}}) \sum_{\mathbf{G}} e^{-G^2/2\beta_0} \{ c(G)[G_2^2 - (G_2^2 G_3^2/\beta_0)] + [dc(G)/dG](G_2^2 G_3^2/G) \} \right]^2}{\left[1 + (1/\rho_0 v_{\text{cell}}) \sum_{\mathbf{G}} e^{-G^2/2\beta_0} c(G)(G_2^2/\beta_0)[1/2(G_3^2/\beta_0) - 1] \right]} \tag{24b}$$

is the contribution from the ϕ part of the dynamical matrix. As expected, the transverse velocity of sound, unlike in the longitudinal velocity, has no contribution from the compressibility. Note that, for small G, the coefficient of $c(G)$ in Eq. (24a) is smaller than its coefficient in Eq. (22a) because G^2/β_0 is much smaller than 1 (as β_0 is large) until the value of $G = q$ where $c(q)$ is appreciably different from zero. However, the coefficients of $d^2c(q)/dq^2$ are comparable. Therefore, the curvature of the direct correlation function plays a more important role in case of transverse mode of vibration than in case of longitudinal mode [where $c(G)$ plays an equally important role]. From the denominators of Eqs. (22b) and (24b), it is difficult to predict whether the correction term is positive or negative because $c(G)$ can be both positive or negative. Our numerical results show that this correction term reduces the velocity of sound. The analogues of the expressions (22) and (24) for other principal directions are not as simple as they are for the (200) direction. However, all trends that we discuss below are similar (such as the dependence of the velocities of sound on the freezing parameters).

Using the structure factors discussed in Sec. III, we obtain the velocities of sound from Eqs. (21) and (23). They are presented in Table II.

The calculated sound velocities are to be compared with those obtained experimentally from ultrasonic measurements:[31] $v_l = 1259$ m s^{-1} and (average) $v_t = 575$ m s^{-1} measured at $T = 83.7$ K [along the (220) direction; the velocities of the two transverse modes T_1 and T_2 are 575 and 571 m s^{-1}, respectively] in solid argon. From this comparison we see that the calculated velocities are larger roughly by a factor of 2 in the longitudinal case and three in the transverse case. From our numerical work we see that the effect of the ϕ part of the dynamical matrix is to reduce the sound velocities. Therefore, it follows that the denominators of Eqs. (22b) and (24b) are positive.

C. Phonon dispersion in solid argon

In this section we discuss the results of our phonon-dispersion calculation. The calculation has been done using all the three sets of structure-factor data for argon discussed in Sec. III (for Yarnell's data we use $N_s = 39$ and 44). Phonon-dispersion curves obtained from our calculations in the (200)-, (220)-, and (111)-symmetry directions are given in Figs. 1 and 7–9. For clarity, as an illustration, the small-q portions of Fig. 1 are magnified and shown in Fig. 10. The experimentally measured phonon energies[32,33] are also shown in these figures. These figures 1 and 7–10 show that our calculations give qualitatively good results. For example, the slopes of our phonon-dispersion curves at $q = 0$ are larger for the longitudinal mode than for the transverse ones along all the three directions. However, there is a quantitative discrepancy between our results and experimental ones: we get larger energies for all wave-vectors in all the directions (for all the sets of structure-factor data we use); the calculated phonon energies, at the zone boundary, for example, are about 1.5 times the experimentally measured phonon energies.

D. Force constants

It is instructive to examine the force constants (i.e., the real-space representation of the dynamical matrix) that result in our theory. These are determined by the Fourier transform of the right-hand side of Eq. (18). However, as discussed earlier, since the contribution to these from the ϕ part (due to the deformation of the Gaussian distributions) is no more than 20%, a reasonable feeling for the

TABLE II. Comparison of freezing parameters (a, α_0, and Lindeman parameter L), of velocities [longitudinal (v_l) and transverse (v_t)], of sound in solid argon between the calculated (present work) and the available experimental measurements at temperatures (third column) close to the triple point. The calculated results have been obtained using the structure factor $S(q)$ (of liquid argon) data measured by (1) Yarnell *et al.* (Ref. 3) ($T=85$ K, $\rho_0=0.021\,25$ Å^{-3}) and (2) Page (Ref. 2) ($T=84.5$ K, $\rho_0=0.021\,29$ Å^{-3}), and (3) on $S(q)$ data set obtained from Goldman's fit to molecular simulation data ($T=107.8$ K, $\rho_0=0.0208$ Å^{-3}, using LJ parameters for argon). The number of reciprocal-lattice-vector (RLV) shells used in each of the calculations is given in the fourth column.

Work	$S(q)$	T (K)	No. of RLV sets	ρ_0 (Å^{-3})	ρ_s (Å^{-3})	a (Å)	α_0	L	v_l (m/s)	v_t (m/s)
Present work	1	85	31	0.021 25		3.79	394.0	0.061 7	2 038	1 638
			39			3.771	526.16	0.053 4	2 403	1 851
			44			3.776	451.41	0.057 6	2 153	1 703
	2	84.5	18	0.021 29		3.815	541.12	0.052 6	2 641	1 749
	3	107.8	50	0.020 8		3.82	278.9	0.073 3	2 131	1 517
Experiment[a]		83		0.022 06	0.024 74	3.852				
Experiment (Ref. 31)		83.7							1 259	575
Experiment (Ref. 15)		94.73			0.024 317	3.874				

[a]From R. K. Crawford and W. B. Daniels, Phys. Rev. Lett. **21**, 367 (1968).

sizes of the force constants can be obtained by neglecting this (second) term in Eq. (18). The force constants corresponding to just the first term in Eq. (18) are given by $H_1^{ij}(\mathbf{R}-\mathbf{R}')$ [cf., Eqs. (7), (10), and (11a)] which corresponds to using $c(|\mathbf{R}-\mathbf{R}'|)$ as an effective interatomic potential [cf. Eqs. (7)–(9)].

We calculate the direct correlation function $c(r)$ from Yarnell's data for $S(q)$ with the following modifications: Yarnell's data extends up to 11.75 Å^{-1}. However, at $q=11.75$ Å^{-1}, $c(q)$ $[=1-1/S(q)]$ is not close to zero. Therefore, we keep Yarnell's data up to $q=11.3$ Å^{-1}, where $c(q)\approx 0$, and set $c(q)=0$ for $q>11.3$ Å^{-1}. Then we obtain $c(r)$ by Fourier transforming $c(q)$. [This choice of $c(q)$ corresponds to our choice of $N_s=39$ in our calculations for freezing parameters (Sec. IV A), velocities of sound (Sec. IV B), and the phonon energies (Sec. IV C).] The direct correlation function $c(r)$ thus obtained is plotted in Figs. 11(a)–11(b). We see that $c(r)$ dies off very rapidly [beyond the distance to third-nearest neighbor of each atom in the crystal, $c(r)$ is almost zero]. We also see from Fig. 11(b) that $c(r)$ is largest (peaked) at distance almost exactly equal to the cell parameter (calculated with $N_s=39$). [This is true when $c(r)$ is calculated taking $N_s=33$ also.] From $c(r)$ [Fig. 11(b)] we calculate the first [Fig. 11(c)] and second [Fig. 11(d)] derivatives of $c(r)$. From Eq. (24) and using the calculated $c(r)$ and its derivatives (Figs. 11), we get the force constants $H_1^{ij}(\mathbf{R})$. We find force constants corresponding to, for example, two nearest neighbors of atoms in the solid are about 4.2×10^3 and 90 dynes/cm, respectively, along the line joining the atoms. We see that the force constants fall off rapidly with increasing R, so that we may set $H_1^{ij}(\mathbf{R})=0$ for R greater than third-nearest-neighbor distance and beyond for solid argon.

As a cross check, we use the force constants at the lattice points $\mathbf{R}'=a(1/\sqrt{2},1\sqrt{2},0)$ and $\mathbf{R}''=a(\sqrt{2},0,0)$ to calculate the phonon energies (the U part of the dynamical matrix to be precise). For simplicity we do the calcu-

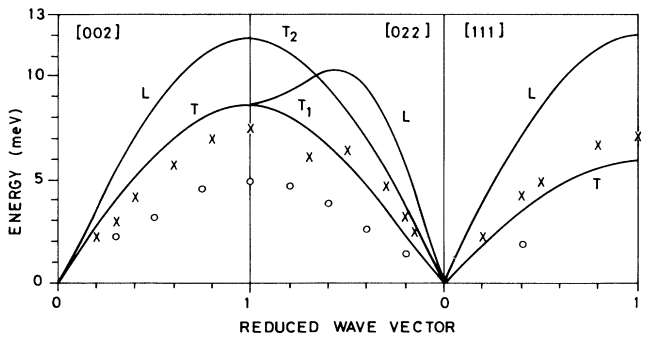

FIG. 7. The same as Fig. 1, but with $N_s=44$.

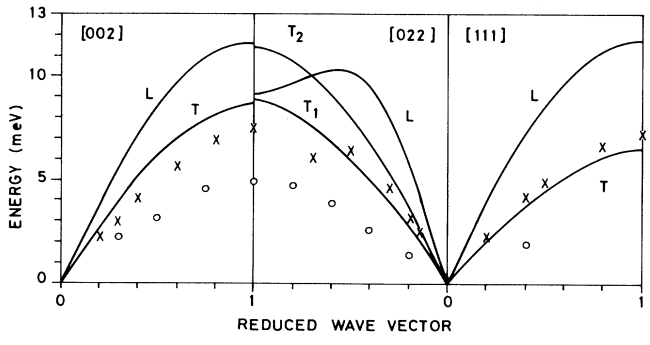

FIG. 8. The same as Fig. 1, but with $n_s=18$ and Page's structure-factor data (fit P_2) instead of the data of Yarnell *et al.*

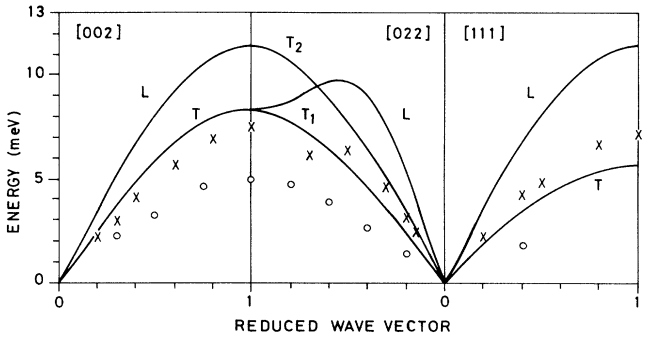

FIG. 9. The same as Fig. 1, but with $N_s=50$ and, instead of the structure-factor data of Yarnell *et al.*, our modification of Goldman's fit (Fig. 3) is used.

lation in the (2,0,0) wave-vector direction; that is, we take our wave vector $\mathbf{k}=(2,0,0)\pi q/a\sqrt{2}$ such that $|\mathbf{k}|$ ranges from the Brillouin-zone center ($q=0$) to the zone boundary ($q=1$). The longitudinal and the transverse elements of the dynamical matrix are, respectively,

$$D_l(\mathbf{k})=-\frac{2}{\beta}\left[4\sin^2(\pi q/2)\left[\frac{1}{R'}\frac{c(R')}{R'}+\frac{\partial^2 c(R')}{\partial R'^2}\right]+2\sin^2(\pi q)\frac{\partial^2 c(R'')}{\partial R''^2}\right] \tag{25}$$

$$D_t(\mathbf{k})=-\frac{2}{\beta}\left[2\sin^2(\pi q/2)\left[\frac{3}{R'}\frac{\partial c(R')}{\partial R'}+\frac{\partial^2 c(R')}{\partial R'^2}\right]+\frac{1}{R''}\sin^2(\pi q)\frac{c(R'')}{R''}\right]. \tag{26}$$

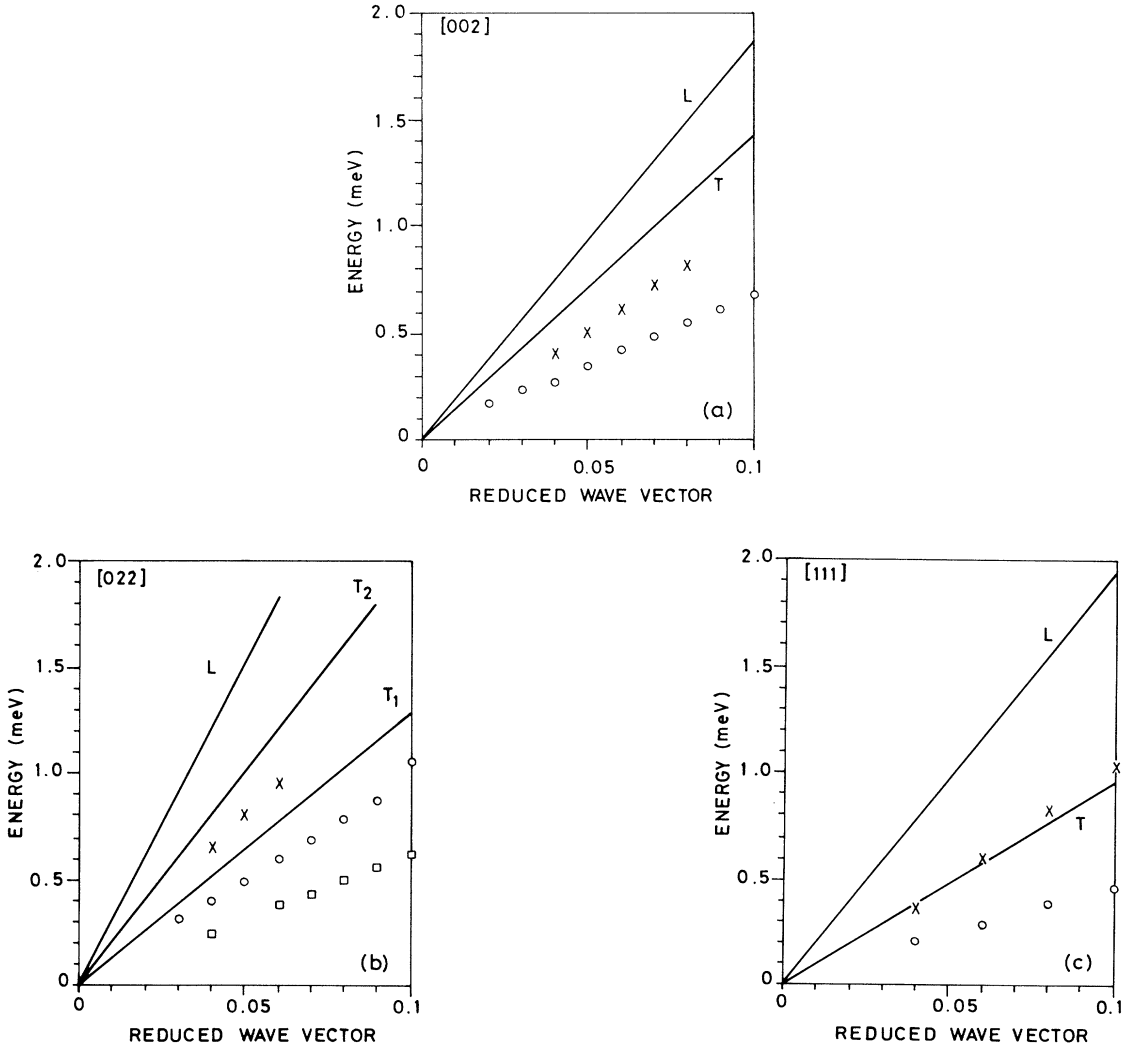

FIG. 10. The small-q part of the phonon-dispersion curves obtained from our calculation. Data are same as in Fig. 1, except for the experimental points, which are taken from the measurements of Fujii *et al.* (Ref. 33). Crosses denote the longitudinal mode, circles the transverse mode T_2, and squares the transverse mode T_1. If T_1 and T_2 are degenerate, then only circles are used.

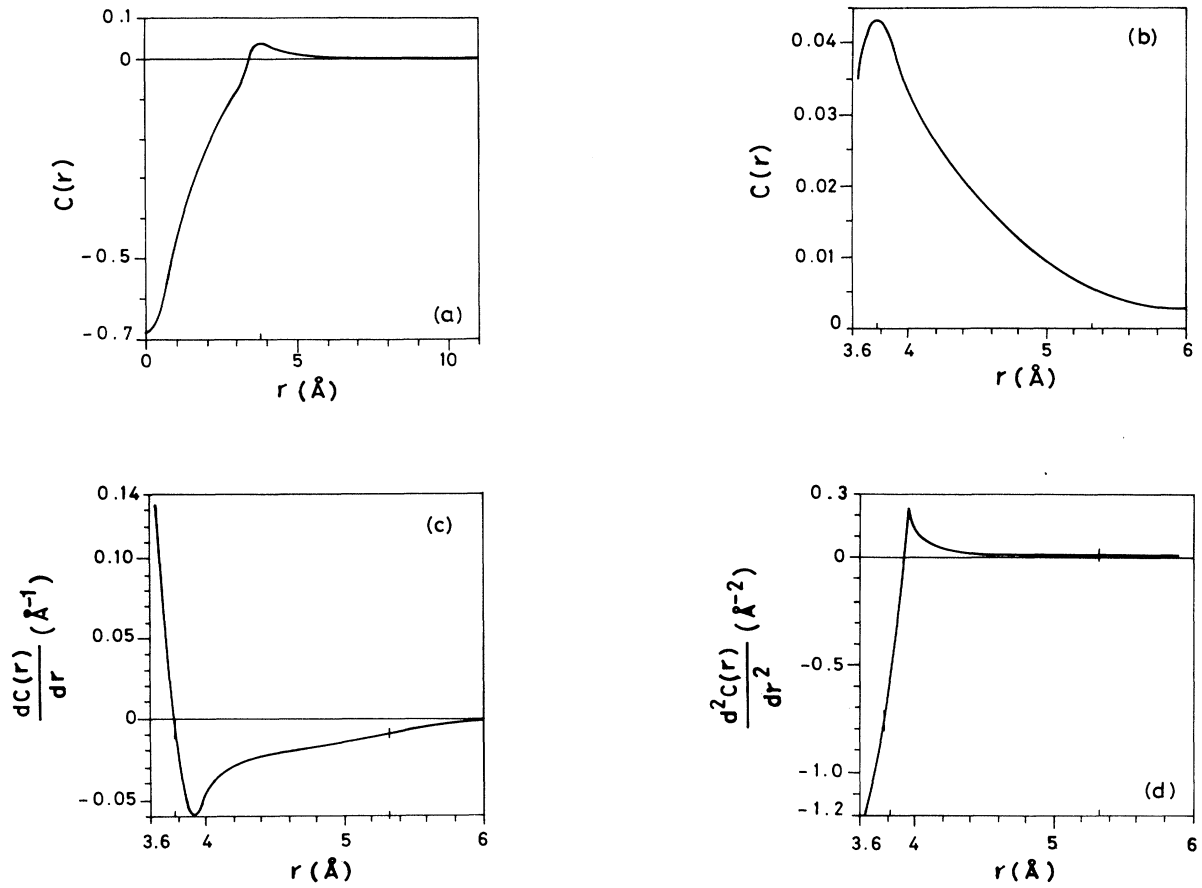

FIG. 11. The direct correlation function $c(r)$ and its first two derivatives as obtained from the structure-factor data of Yarnell *et al.* (Ref. 24) and with $N_s = 39$ (used in our calculation of a and α_0). (a) The direct correlation function $c(r)$ with $0 \leq r \leq 11.0$ Å, (b) an expanded view of the peak of $c(r)$,(c) the first derivative of $c(r)$ [same scale as in (b)] (d) the second derivative of $c(r)$ [same scale as in (b)]. The distances $r\,(=R)$ at which the force constants are calculated are shown in (c) and (d) by small (vertical) markings.

We find that this calculation yields phonon energies larger than what the full correlation function [the U part of Eq. (18)] gives.

From the derivatives of $c(r)$ we see that $d^2c(R)/dR^2$ has opposite sign at the two lattice sites and the term outside the large parentheses in Eq. (25) reduces the phonon frequencies, but the term outside the large parentheses in Eq. (26) increases frequencies. Therefore, we see that many more force constants have to be included to calculate the phonon frequencies.

V. DISCUSSION

From Sec. IV we have seen that, while our calculations yield qualitatively reasonable results, quantitatively the results compare poorly with the experimental data. The calculated velocities of sound differ from the observed velocities by a factor of about 2 and phonon energies at the zone boundaries differ from the experimental values by roughly a factor of 1.5. In this section we discuss the reasons for this poor agreement, and argue that our method is viable and can provide much better results with improved inputs.

The point is that there are three major simplifying approximations we have made in the calculations we presented in this paper. (1) We have chosen the specific approximate density functional (of Ramakrishnan and Yussouff) obtained by truncating the free-energy functional at second order. (2) We have used an approximate parametrization of the local density as a sum of nonoverlapping Gaussians, and further simplified by assuming zero-vacancy concentration. (3) We have used approximate inputs for the structure-factor–direct-correlation-function data. Each of these is responsible, to different extents, for the poor agreement between theory and experiment.

To begin with, note that the poor agreement with experimental data also characterizes our freezing parameters. All our calculated values for the cell parameter a are too small compared to experiment and the calculated Lindeman ratio is also smaller roughly by a factor of 2

(see Table II). By the same token, the smallest reciprocal-lattice vector G_0 ($=2.04$ Å^{-1} for Yarnell's data with $N_s=39$, for example) of the solid, determined by the cell parameter a, does not fall at the first peak q_0 [$=1.992$ in Yarnell's $S(q)$ data] of the structure factor $S(q)$, but at a higher value of the wave vector (i.e., $G_0 > q_0$). (For comparison, the experimental value of the smallest reciprocal-lattice vector of an argon[15] crystal at 83.17 K is 1.991 Å^{-1}.) Thus, our calculated solid is much denser than the real one, and hence it is not surprising that it will appear stiffer, with higher phonon frequencies than the real one. Similar features characterize the recent study by Jaric and Mohanty[18] where they calculate the elastic constants of a Lennard-Jones system using approximations similar to the above; their results are quantitatively as inadequate as ours.

In order to bring out this point better, it is instructive to make a (*ad hoc*) calculation of the sound velocities at values of the cell parameter held fixed at values larger than what we have (so that $G_0 \to q_0$), and minimize only with respect to α_0. For these calculations we have used Yarnell's data with $n_s=39$ and $N_s=44$, Page's data with $N_s=18$, and our modified version of Goldman's fit (Sec. III B) with $N_s=50$. All these sets of data yield similar trends in the variations of the velocities of sound with G_0, therefore, we present the results obtained for Yarnell's data with $N_s=39$.

In Figs. 12(a)–12(d), we show how the velocities of sound, etc., vary as we make $G_0 \to q_0$, thus expanding our crystal, which is parametrized as in Eq. (5). (This expansion is carried out with a fixed direct correlation function, i.e., with fixed temperature and pressure.) The range of q over which G_0 is varied to obtain the results of Figs. 12(a)–12(d) is shown in Fig. 13. Figure 12(a) shows the variations of the sound velocities with G_0; Fig. 12(b) shows the corresponding variation of the sound velocities, when the Gaussian density distributions are not allowed to deform. The values of the free energy (minimized only with respect to α_0) are plotted in Fig. 12(c), and the values of α_0 at the minima are plotted against G_0 in Fig. 12(d). We see the following from these figures: (1) The velocities v_l and v_t decrease as G_0 decreases. The

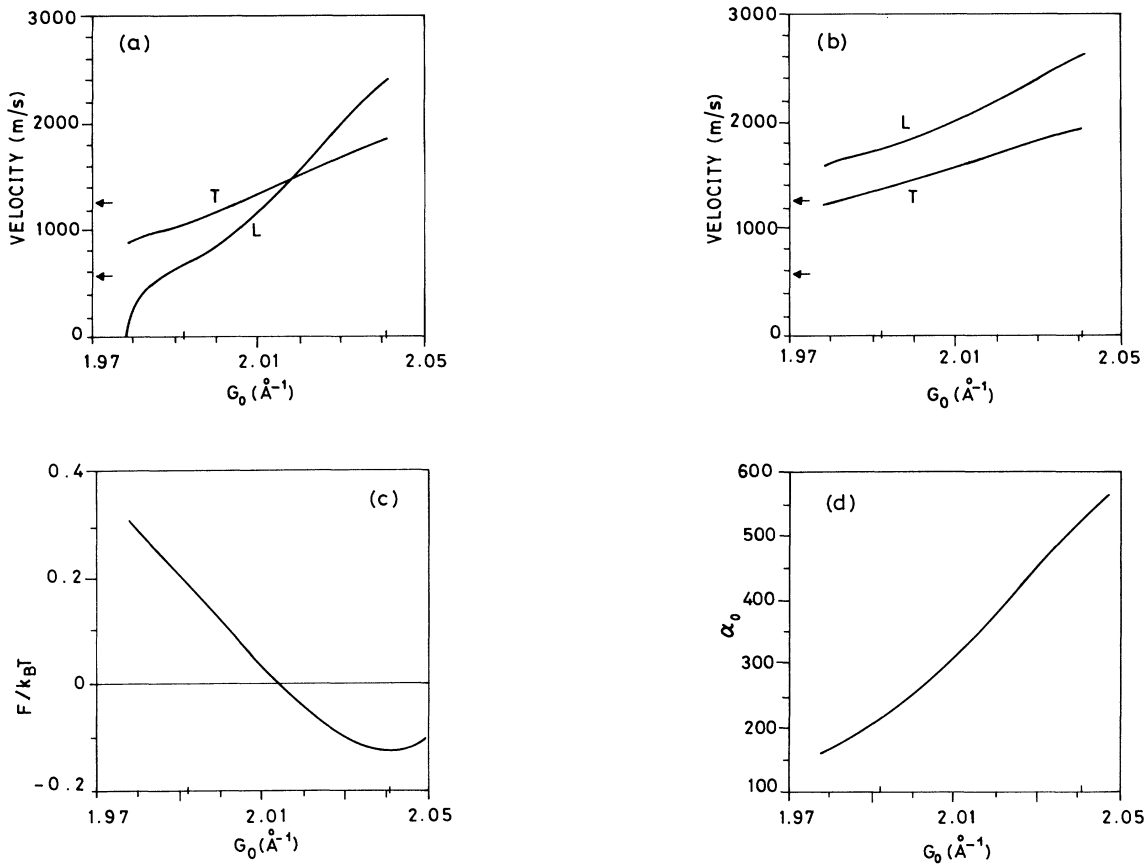

FIG. 12. The variation with G_0 (the magnitude of the smallest reciprocal-lattice vector) of (a) the velocities of sound, both longitudinal (v_l) and transverse (v_t) in the (200) direction [the experimental values (Ref. 31) are indicated by arrows on the vertical axis], (b) the contributions to v_l and v_t from the U part of the dynamical matrix (see text), (c) the free-energy functional minimized with respect to the width parameter α_0, (d) the value of α_0 at this minimum. We use the structure-factor $S(q)$ data of Yarnell *et al.* (Ref. 24) for these figures and set $N_s=39$. [The largest peak position of $S(q)$ and G_0 at which F has a global minimum are marked on the horizontal axis.]

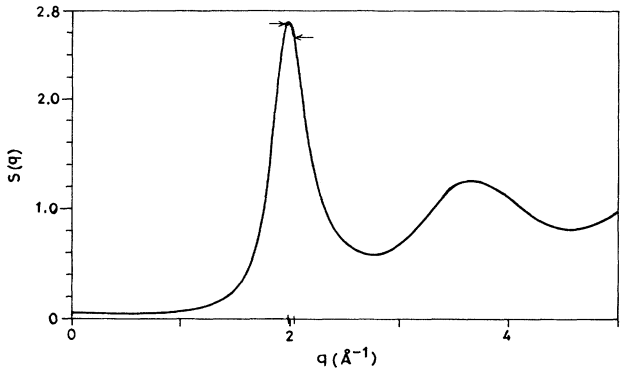

FIG. 13. The structure-factor data of Yarnell *et al.* (Ref. 24) on an expanded scale (cf. Fig. 2) showing (by arrows) the range over which G_0 is varied to obtain the plots of Fig. 12. (The arrow tip positions are marked on the horizontal axis also.)

variation of v_l with G_0 is more dramatic than that of v_t: with decreasing G_0, v_l becomes smaller than v_t and ultimately becomes zero and then purely imaginary. (2) The ϕ part (the second term) of the dynamical matrix [Eq. (18)] plays an important role in decreasing v_l, as G_0 gets close to q_0. (3) α_0 decreases rapidly as G_0 approaches q_0. It is clear from these results that the velocities of sound depend very sensitively on the cell parameter a.

Similarly, we have calculated the variation of phonon energies with G_0 along the (200)-symmetry direction. The results are shown in Figs. 14(a)–14(c) (from $q=0$ to the Brillouin-zone boundary) and Figs. 15(a)–15(c) (for small q) for three typical values of G_0. From Figs. 14 and 15 we see that the phonon energies decrease with decreasing G_0 for all values of q, so that our phonon dispersion curves move closer to the experimentally observed ones. Note that the slopes of the phonon dispersion curves (Figs. 14) increase (with decreasing G_0) at values of q

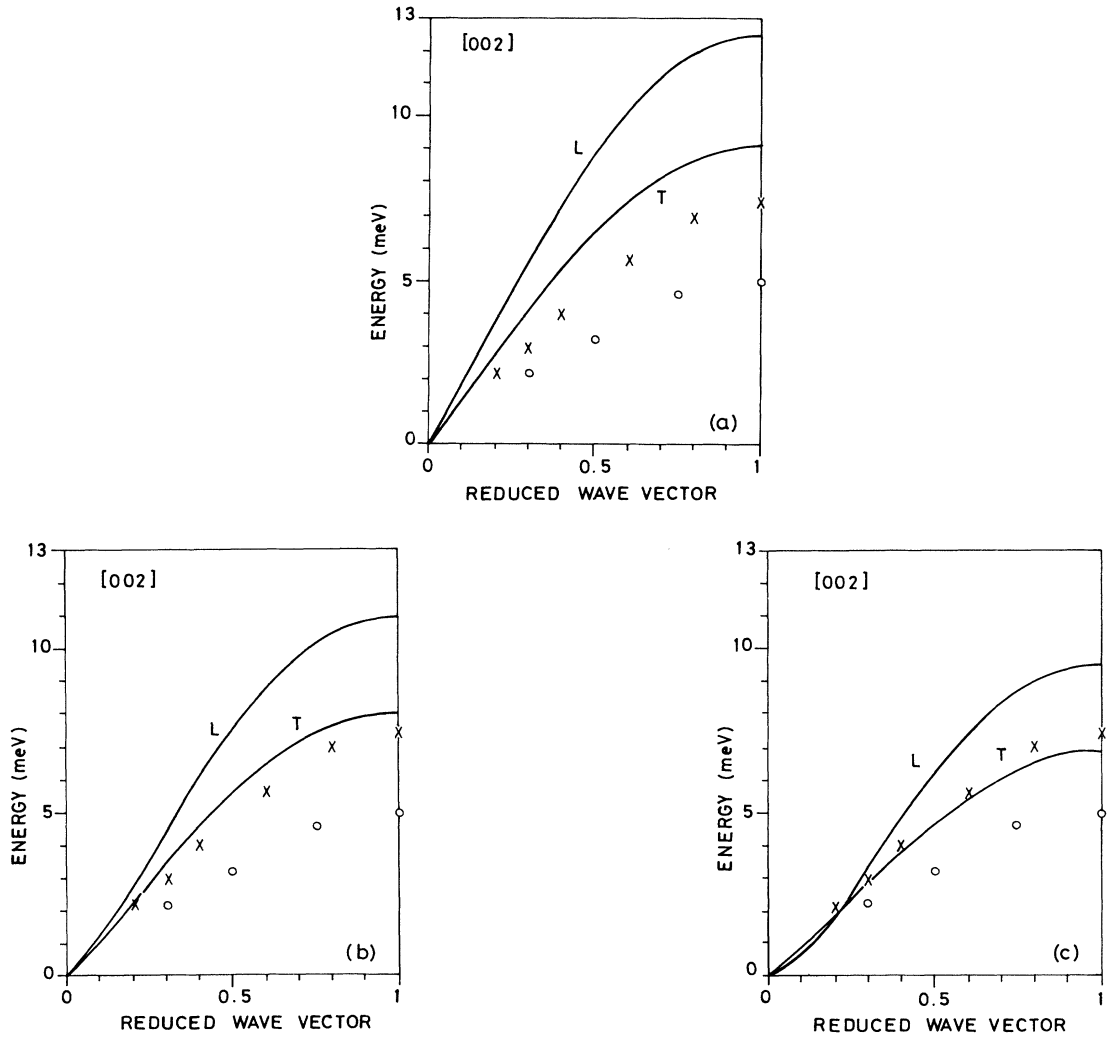

FIG. 14. The variation with G_0 (the magnitude of the smallest reciprocal-lattice vector) of the phonon-dispersion curves [direction (200)] of Fig.1. (In the calculation for this figure, the free energy is minimized only with respect to the width parameter α_0; see text.) (a) $G_0=2.04$ Å^{-1}, (b) $G_0=2.02$ Å^{-1}, (c) $G_0=2.0$ Å^{-1}. The experimental data are the same as in Fig. 1.

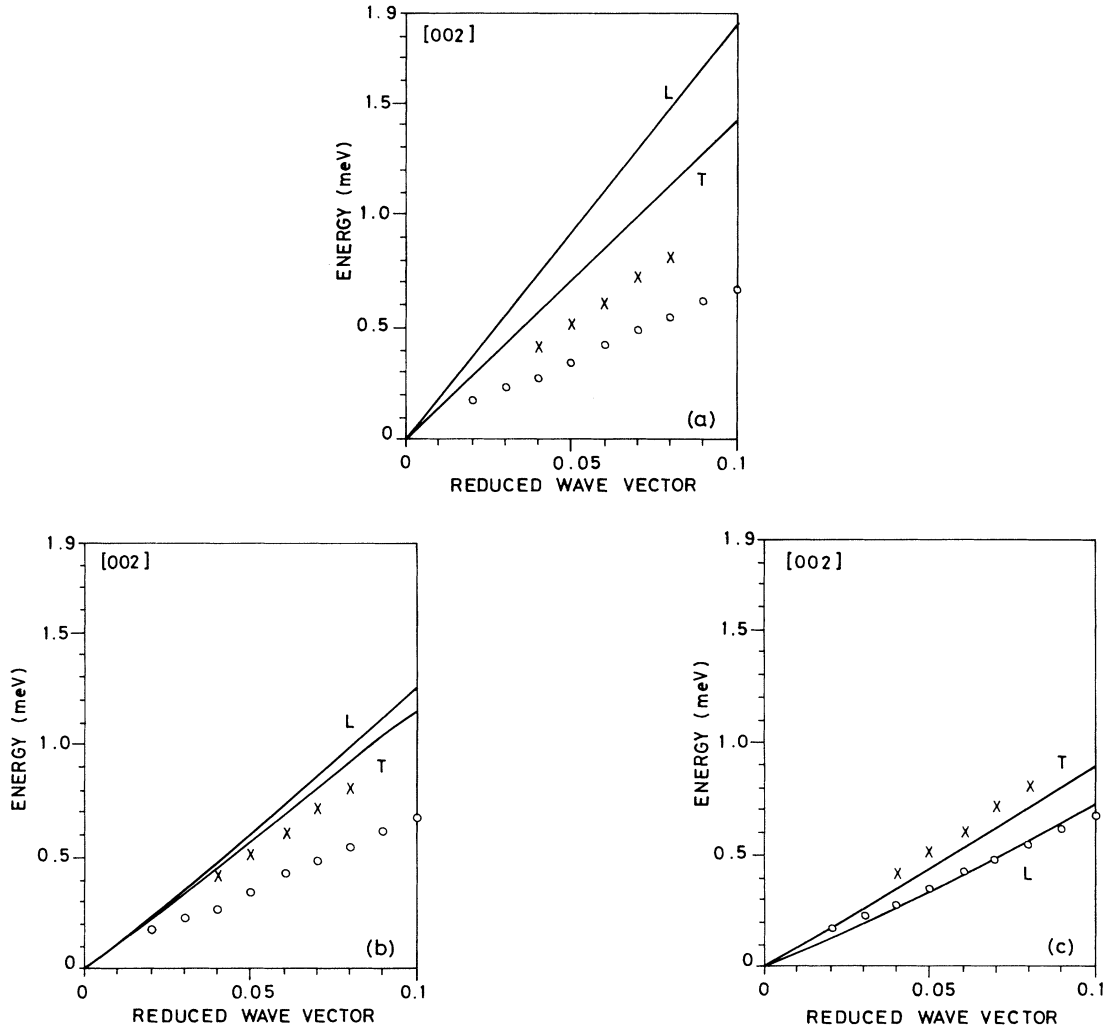

FIG. 15. The small-q parts of the phonon-dispersion curves of Fig. 14. The experimental data are the same as in Fig. 10.

beyond the midpoint between $q=0$ and the zone boundary. This increase is more pronounced as $G_0 \rightarrow q_0$. This is because the period of the ϕ part (which decrease phonon energies) of the dynamical matrix is twice that of the U part. [This follows from the terms ε_1, ε_2, and ε_3 of Eq. (20).] Thus, the reduction of phonon energies because of the ϕ part is zero at $q=0$ and at the Brillouin-zone boundaries, and it is a maximum in between. Therefore, the increase in slope is the maximum just beyond the values of q half-way between $q=0$ and the Brillouin-zone boundary. From Fig. 14(c) we also see that the phonon energies of the longitudinal mode of vibration are smaller than those of the transverse modes for small values of q. This is easily seen from Fig. 15(c). This is because of the increasing contribution of the ϕ part as $G_0 \rightarrow q_0$ [cf., Figs. 12(a) and 12(b)].

It is known in the context of the self-consistent Debye model of a crystal that the Debye temperature Θ_D plays the same role as the Gaussian width α_0 of the crystalline density profile and the two are related as $(\Theta_D/T)=\Lambda\sqrt{3\beta_0/\pi}$, where Λ is the thermal de Broglie wavelength.[34] This observation and the calculations described above suggest that whatever approximations are causing the Lindeman ratio L ($\propto 1/\sqrt{\beta_0}$) to be too small by a factor of 2 also cause the speed of sound ($\propto \Theta_D$) and, presumably, the entire phonon spectrum to be too large by a factor of 2.

First consider the partial extent to which the Gaussian representation for the local density that we use is responsible for the discrepancy. A rough estimate of this can be made from the work of Laird, McCoy, and Haymet,[35] who study the freezing of Lennard-Jones systems using essentially the same free-energy functional and the same input for the liquid correlation functions as one of the ones we use (namely, the one calculated from Goldman's empirical fit to the numerical pair-correlation function for LJ systems; see Sec. III B); for they use the Fourier components of the density as the variational parameters. The freezing parameters and the Lindeman ratios they find, which are listed in Table III, are a little better than

TABLE III. Comparison of the densities (ρ_0 and ρ_s), the cell parameter a, and the Lindeman parameter L at temperatures (third column) close to melting obtained for argon in various density-functional theories. The functional used (first column), input correlation functions (second column), and the model for the solid density (fourth column) are indicated. ε and σ are the LJ parameters for argon. The abbreviations used (also in the text) are as follows: HO, Haymet and Oxtoby; RY, Ramakrishnan and Youssouff; EKP, Ebner, Krishnamurthy, and Pandit; WDA, weighted density approximation; MWDA, modified WDA; MF, mean field; MC, Monte Carlo; ZH, Zerah and Hansen; LJ, Lennard-Jones; LJT, truncated LJ; PY, Percus-Yevic; and HS, hard-sphere systems.

Functional/Method	Correlation Function	k_BT/ε	Approx. for $\rho(r)$	$\rho_0\sigma^{-3}$	$\rho_s\sigma^{-3}$	a/σ	L
HO/RY (Ref. 37)	ZH (Ref. 38) for LJ	1.0	Gaussian	0.974	1.094	1.089	0.105
EKP (Ref. 39)	ZH (Ref. 39) for LJ	1.0	Gaussian	0.944	1.084	1.06	0.12
MWDA+MF (Ref. 37)	ZH for LJT+MF correction for LJ	1.0	Gaussian	0.88	1.025	1.113	0.100
WDA (Ref. 11)	PY for HS+approx.	0.75	Gaussian	0.855	0.970	1.134	0.127
	corrected for LJ	1.15	Gaussian	0.934	1.026	1.113	0.126
HO/RY (Ref. 35)	Goldman's fit (Ref.	1.0	Gaussian	0.88	1.020	1.115	0.074
	27) [c_0 and $c^{(3)}$ (0,0)	1.15	Gaussian	0.918	1.050	1.104	0.074
	from Ref. 30]	0.72	Fourier	0.78	0.954	1.140	0.083
		1.0	expansion	0.877	1.017	1.116	0.086
		1.15		0.916	1.047	1.105	0.087
MC [by Hansen and Verlet as quoted		0.75		0.875	0.973	1.133	0.145
in Ref. 11. The values for $k_BT/\varepsilon=1$		1.0		$\approx$0.91	$\approx$1.005	1.121	
are extrapolated ones [Ref. 39]		1.15		0.936	1.024	1.114	0.139

the ones we get using the simpler Gaussian parametrization of the density, but only by about 15%.

This suggests as the more important culprits (1) our choice for the density functional and (3) the inputs that we use for the liquid correlation functions. Again one gets a feeling as to their relative degrees of responsibility by examining the results from the various density-functional studies of freezing of LJ systems, some of which are listed in Table III. Curtin and Ashcroft[11] obtain a phase diagram and Lindeman ratios for LJ systems that are in good agreement with experiments and computer simulations using a weighted-density-approximation (WDA) functional, which, however, is much more complicated and harder to work with than the simpler Ramakrishnan-Yussouff functional we use here. Denton and Ashcroft[36] have studied a modified WDA (MWDA) functional of a similar sort which is simpler and again obtain reasonable results. These relative merits of the various functionals has been studied extensively in a recent paper by de Kuijper *et al.*[37] They point out, however, that the use of the improved LJ correlation functions obtained from the Zerah and Hansen[38] (ZH) closure scheme, even in the context of the simple RY density functional, gives greatly improved results for the freezing parameters. Finally, Ebner, Krishnamurthy, and Pandit[40] (EKP), in a recent paper, have employed a slightly modified version of the RY density functional that retains its essential simplicity, the ZH correlation functions for the LJ system and the Gaussian representation for the density to obtain results as good as those obtained using the much more complicated WDA. These recent results, summarized in Table III, make it seem likely to us that even the simplest RY functional and the Gaussian representation that we have used here may lead to improved results for the phonon spectra if we were to use better inputs (such as the ones from the ZH scheme) for the liquid correlation functions. Needless to say, for complete agreement of the calculated phonon spectra with the experimental data, use of one of the improved density functionals and calculations improving upon[41] the Gaussian approximations may be necessary. We are presently investigating these issues and hope to present the results elsewhere. In the meanwhile, poor agreement with experiment notwithstanding, we believe that the calculations we have presented here and the insights they provide into phonon spectra of crystals close to melting and their relation to liquid correlation functions are of scientific value.

ACKNOWLEDGMENTS

One of the authors (M.C.M.) wishes to thank R. Pandit and M. Rao for discussion and encouragement. We thank the Council of Industrial and Scientific Research, India, and the Department of Science and Technology, India, for financial support.

APPENDIX A: LATTICE VIBRATION WITHOUT DISTORTION OF GAUSSIAN DENSITY DISTRIBUTIONS

The RY density functional [Eq. (1) with $c^n=0$ for $n\geq 3$] for the excess free energy of a solid with local density $\rho(\mathbf{r})$ can be written as

$$\beta F_0=\beta F_{\text{ent}}+\beta F_{\text{int}}\ , \tag{A1}$$

where

$$\beta F_{\text{ent}}=\int d\mathbf{r}\,\rho(\mathbf{r})\ln\left[\frac{\rho(\mathbf{r})}{\rho_0}\right]-\int d\mathbf{r}[\rho(\mathbf{r})-\rho_0] \tag{A2}$$

is defined to be the entropic part and

$$\beta F_{\rm int}=-\tfrac{1}{2}\int d\mathbf{r}_1\int d\mathbf{r}_2\, c(|\mathbf{r}_1-\mathbf{r}_2|)[\rho(\mathbf{r}_1)-\rho_0]\times[\rho(\mathbf{r}_2)-\rho_0] \tag{A3}$$

is the interaction part. For a crystal where each of the lattice sites is occupied by one atom (i.e., ignoring vacancies), the Gaussian parametrization of the local density can be written [cf., Eq. (5)] as

$$\rho(\mathbf{r})=(\beta_0/\pi)^{3/2}\sum_{\mathbf{R}} e^{-\beta_0(\mathbf{R}-\mathbf{r})^2}, \tag{A4}$$

where $\beta_0=\alpha_0/a^2$. With this form of $\rho(\mathbf{r})$, and neglecting overlap between the Gaussians centered at different sites, we evaluate (A2) and (A3) separately and get

$$\frac{\beta F_{\rm ent}}{N}=\ln[(\beta_0/\pi)^{3/2}]-\tfrac{5}{2}-\ln\rho_0+\rho_0 v_{\rm cell}, \tag{A5}$$

$$\frac{\beta F_{\rm int}}{N}=-\frac{1}{2\rho_0 v_{\rm cell}}\sum_{\mathbf{G}} e^{-G^2/2\beta_0}c(G)+c_0-\tfrac{1}{2}\rho_0 c_0 v_{\rm cell}, \tag{A6}$$

where $c(q)=\rho_0\int d\mathbf{r}\, c(r)e^{i\mathbf{q}\cdot\mathbf{r}}$, $c(G)=c(q=G)$, and $c_0=c(q=0)$. **G**'s are the reciprocal-lattice vectors of the crystal. N is the number of lattice sites in the crystal $v_{\rm cell}=a^3/\sqrt{2}$ is the volume of each primitive cell of the crystal. Hence, the expression (6) for $\beta F_0/N$.

When the average position of the atoms are displaced by $\mathbf{u}(\mathbf{R})$, we parametrize $\rho(\mathbf{r})$ as a sum of Gaussian density distributions centered at $\mathbf{R}+\mathbf{u}(\mathbf{R})$, i..e,

$$\rho(\mathbf{r})=(\beta_0/\pi)^{3/2}\sum_{\mathbf{R}} e^{-\beta_0[\mathbf{R}+\mathbf{u}(\mathbf{R})-\mathbf{r}]^2}, \tag{A7}$$

in place of Eq. (A4). If we assume that the displacements $\mathbf{u}(\mathbf{R})$ are small, and neglect terms of $O(u^3)$ and higher,

$$\rho(\mathbf{r})=(\beta_0/\pi)^{3/2}\times\sum_{\mathbf{R}} e^{-\beta_0(\mathbf{R}-\mathbf{r})^2}\{1-2\beta_0\mathbf{u}(\mathbf{R})\cdot(\mathbf{R}-\mathbf{r})-\beta_0 u^2(\mathbf{R})+2\beta_0^2[\mathbf{u}(\mathbf{R})\cdot(\mathbf{R}-\mathbf{r})]^2\}. \tag{A8}$$

In an approximation where we neglect the overlap between the Gaussian density distribution functions centered at different lattice sites $\beta F_{\rm ent}$ is still given by (A4). But $\beta F_{\rm int}$ is modified as

$$-2\beta F_{\rm int}=(\beta_0/\pi)^3\sum_{\mathbf{R}_1}\sum_{\mathbf{R}_2}\int d\mathbf{r}_1\int d\mathbf{r}_2\, c(|\mathbf{r}_1-\mathbf{r}_2|)e^{-\beta_0(\mathbf{R}_1-\mathbf{r}_1)^2}e^{-\beta_0(\mathbf{R}_2-\mathbf{r}_2)^2}+\sum_{\mathbf{R}}\sum_{\mathbf{R}'}\sum_i\sum_j u_i(\mathbf{R}')u_j(\mathbf{R}+\mathbf{R}')\left[-\sum_{\mathbf{R}_1}\frac{\partial^2 f(\mathbf{R}_1)}{\partial R_{1i}\,\partial R_{1j}}\delta_{R,0}+\frac{\partial^2 f(\mathbf{R})}{\partial R_i\,\partial R_j}\right]-2Nc_0+c_0\rho_0 V_{\rm solid}, \tag{A9}$$

where

$$f(\mathbf{R})\equiv f(\beta_0,\mathbf{R})=(\beta_0/2\pi)^{3/2}\int d\mathbf{r}\, c(r)e^{-\beta_0(\mathbf{R}-\mathbf{r})^2/2}. \tag{A10}$$

The derivative with respect to **R** is taken assuming **R** to be a continuous independent variable, such that

$$\frac{\partial f(\mathbf{R})}{\partial R_i}=(\beta_0/2\pi)^{3/2}\times\int d\mathbf{r}\, e^{-\beta_0(\mathbf{R}-\mathbf{r})^2/2}c(r)(-\beta_0)(\mathbf{R}-\mathbf{r})_i,$$

etc. (In our numerical calculations all derivatives are evaluated in reciprocal space.)

Hence, the change in the free energy ΔF of the solid because of the displacements $\mathbf{u}(\mathbf{R})$ is entirely due to the interaction part and is given by Eq. (7),

$$\beta\Delta F=\beta(F-F_0)=\tfrac{1}{2}\sum_{\mathbf{R}}\sum_{\mathbf{R}'}\sum_i\sum_j u_i(\mathbf{R}')u_j(\mathbf{R}+\mathbf{R}')\times\left[\sum_{\mathbf{R}_1}\frac{\partial^2 f(\mathbf{R}_1)}{\partial R_{1i}\,\partial R_{1j}}\delta_{R,0}-\frac{\partial^2 f(\mathbf{R})}{\partial R_i\,\partial R_j}\right]. \tag{A11}$$

APPENDIX B: LATTICE VIBRATION WITH DISTORTION OF GAUSSIAN DENSITY DISTRIBUTIONS

To allow for a deformation of the Gaussian density distributions, we extend Eq. (A8) as follows:

$$\rho(\mathbf{r})=\sum_{\mathbf{R}}\frac{(\det\{\beta_0[1+\boldsymbol{\alpha}(\mathbf{R})]\})^{1/2}}{\pi^{3/2}}\exp\{[\mathbf{R}+\mathbf{u}(\mathbf{R})-\mathbf{r}]_i[\delta_{ij}+\alpha_{ij}(\mathbf{R})][\mathbf{R}+\mathbf{u}(\mathbf{R})-\mathbf{r}]_j\}, \tag{B1}$$

where the Gaussian width parameter α_0 $(=a^2\beta_0)$ is replaced here by $\alpha_0[1+\boldsymbol{\alpha}(\mathbf{R})]$, 1 is a 3×3 unit matrix, and $\boldsymbol{\alpha}(\mathbf{R})$ is a 3×3 symmetric matrix. We assume the elements $\alpha_{ij}(\mathbf{R})\approx O(u)$, and we check this self-consistently within our calculations. Thus, to $O(u^2)$

$$\rho(\mathbf{r})=(\beta_0/\pi)^{3/2}\sum_{\mathbf{R}}\exp[\tfrac{1}{2}(\mathrm{Tr}\boldsymbol{\alpha}(\mathbf{R})-\tfrac{1}{2}\mathrm{Tr}\boldsymbol{\alpha}^2(\mathbf{R})] \times\exp\left[-\alpha_0\left[(\mathbf{R}-\mathbf{r})^2+2\sum_i(\mathbf{R}-\mathbf{r})_i u_i(\mathbf{R})+u^2(\mathbf{R}) +\sum_{i,j}(\mathbf{R}-\mathbf{r})_i\alpha_{ij}(\mathbf{R})(\mathbf{R}-\mathbf{r})_j+2\sum_{i,j}(\mathbf{R}-\mathbf{r})_i\alpha_{ij}(\mathbf{R})u_j(\mathbf{R})\right]\right] . \tag{B2}$$

We further expand the exponentials, retain terms up to quadratic order in $\mathbf{u}(\mathbf{R})$ and $\alpha_{ij}(\mathbf{R})$, and calculate the free-energy functional (A1). Again, we assume that the overlap between the Gaussian density distributions at different sites is negligible. After the evaluation of the Gaussian integrals we get

$$\beta F_{\mathrm{ent}}=N\ln[(\beta_0/\pi)^{3/2}]-5N/2-N\ln\rho_0+\rho_0 V_{\mathrm{solid}}+\sum_{\mathbf{R}}\sum_{\substack{i,j\\k,n}}[-\tfrac{1}{8}(\delta_{in}\delta_{jk}+\delta_{ik}\delta_{jn})]\alpha_{ij}(\mathbf{R})\alpha_{kn}(\mathbf{R}) . \tag{B3}$$

Since $\alpha_{ij}(\mathbf{R})$ can be both positive and negative, we have used $\sum_{\mathbf{R}}\alpha_{ij}(\mathbf{R})=0$. As is clear from Eqs. (A6) and (B3), the entropic part of βF changes only because of the deformation of the Gaussian density distributions. This change is

$$\beta\Delta F_{\mathrm{ent}}=-\sum_{\mathbf{R}}\sum_i\sum_j\tfrac{1}{4}\alpha_{ij}^2(\mathbf{R}) .$$

Similarly we find

$$\beta F_{\mathrm{int}}=-\tfrac{1}{2}(\beta_0/\pi)^{3/2}\sum_{\mathbf{R}_1}\sum_{\mathbf{R}_2}\int d\mathbf{r}_1 d\mathbf{r}_2 c(|\mathbf{r}_1-\mathbf{r}_2|)e^{-\beta_0(\mathbf{R}_1-\mathbf{r}_1)^2}e^{-\beta_0(\mathbf{R}_2-\mathbf{r}_2)^2}+Nc_0-\tfrac{1}{2}c_0\rho_0 V_{\mathrm{solid}}$$
$$+\tfrac{1}{2}\sum_{\mathbf{R}}\sum_{\mathbf{R}'}\left[\sum_{i,j}u_i(\mathbf{R}')u_j(\mathbf{R}+\mathbf{R}')\left[-\sum_{\mathbf{R}_1}\frac{\partial^2 f(\mathbf{R}_1)}{\partial R_{1i}\partial R_{1j}}\delta_{R,0}+\frac{\partial^2 f(\mathbf{R})}{\partial R_i\partial R_j}\right]\right.$$
$$+\sum_{i,j,k}u_i(\mathbf{R}')\alpha_{jk}(\mathbf{R}+\mathbf{R}')\left[-\frac{1}{4\beta_0}\frac{\partial^3 f(\mathbf{R})}{\partial R_i\partial R_j\partial R_k}-\frac{1}{4\beta_0}\sum_{\mathbf{R}_1}\frac{\partial^3 f(\mathbf{R}_1)\delta_{R,0}}{\partial R_{1i}\partial R_{1j}\partial R_{1k}}\right]$$
$$+\sum_{i,j,k}\alpha_{ij}(\mathbf{R}')u_k(\mathbf{R}+\mathbf{R}')\left[\frac{1}{4\beta_0}\frac{\partial^3 f(\mathbf{R})}{\partial R_i\partial R_j\partial R_k}-\frac{1}{4\beta_0}\sum_{\mathbf{R}_1}\frac{\partial^3 f(\mathbf{R}_1)\delta_{R,0}}{\partial R_{1i}\partial R_{1j}\partial R_{1k}}\right]$$
$$+\sum_{\substack{i,j,\\k,n}}\alpha_{ij}(\mathbf{R}')\alpha_{kn}(\mathbf{R}+\mathbf{R}')$$
$$\times\left\{-\delta_{R,0}\left[\frac{1}{16\beta_0^2}\sum_{\mathbf{R}_1}\frac{\partial^4 f(\mathbf{R}_1)}{\partial R_{1i}\partial R_{1j}\partial R_{1k}\partial R_{1n}}\right.\right.$$
$$+\frac{1}{8\beta_0}\sum_{\mathbf{R}_1}\left[\frac{\partial^2 f(\mathbf{R}_1)}{\partial R_{1j}\partial R_{1n}}\delta_{ik}+\frac{\partial^2 f(\mathbf{R}_1)}{\partial R_{1j}\partial R_{1k}}\delta_{in}\right.$$
$$\left.\left.\left.+\frac{\partial^2 f(\mathbf{R}_1)}{\partial R_{1i}\partial R_{1n}}\delta_{jk}+\frac{\partial^2 f(\mathbf{R}_1)}{\partial R_{1i}\partial R_{1k}}\delta_{jn}\right]\right]-\frac{1}{16\beta_0^2}\frac{\partial^4 f(\mathbf{R})}{\partial R_i\partial R_j\partial R_k\partial R_n}\right\}\Bigg], \tag{B4}$$

where $f(\mathbf{R})$ is defined in Eq. (A10). From these it is easily verified that the total change in free energy as a result of the displacements of atoms (including the deformations of the Gaussian density distributions) given by

$$\beta\Delta F=\beta(F-F_0)=\beta(F_{\mathrm{ent}}+F_{int}-F_0)$$

can be written in the form (10) with $\mathbf{H}_i$'s as given by Eqs. (11a)–(11d) of the text.

APPENDIX C: DYNAMICAL MATRIX

Minimizing the change in the free energy [Eq. (15), Sec. II] with respect to the ϕ_σ's [related to the α_{ij}'s (Table II)], we get

$$\frac{\partial(\beta\Delta F)}{\partial\phi_\sigma(\mathbf{R}_1)}=\sum_{\mathbf{R}}\left[\sum_{i=1}^{3}u_i(\mathbf{R}_1-\mathbf{R})F_2^{i\sigma}(\mathbf{R})+\sum_{i=1}^{3}F_3^{\sigma i}(\mathbf{R})u_i(\mathbf{R}+\mathbf{R}_1)+\sum_{\mu=1}^{6}F_4^{\sigma\mu}(\mathbf{R})\phi_\mu(\mathbf{R}+\mathbf{R}_1)+\sum_{\mu=1}^{6}\phi_\mu(\mathbf{R}_1-\mathbf{R})F_4^{\mu\sigma}(\mathbf{R})\right]$$
$$=0\ . \tag{C1}$$

Since the $\mathbf{R}$'s are the lattice vectors of the crystal, a Fourier transform of Eq. (C1) yields

$$\sum_i[u_i(\mathbf{q}_1)E_2^{i\sigma}(\mathbf{q}_1)+E_3^{\sigma i}(\mathbf{q}_1)u_i(\mathbf{q}_1)]+\sum_\mu[E_4^{\sigma\mu}(-\mathbf{q}_1)\phi_\mu(\mathbf{q}_1)+\phi_\mu(\mathbf{q}_1)E_4^{\mu\sigma}(\mathbf{q}_1)]=0\ ,$$

where $E_1^{ij}(\mathbf{q})=\sum_{\mathbf{R}}F_1^{ij}(\mathbf{R})e^{i\mathbf{q}\cdot\mathbf{R}}$, etc. These are readily solved for $\phi_\mu(\mathbf{q})$ to get

$$\phi_\mu(\mathbf{q})=-\sum_i\sum_\sigma u_i(\mathbf{q})E_2^{i\sigma}(\mathbf{q})[E_4^{-1}(\mathbf{q})]^{\sigma\mu}$$
$$=-\sum_\sigma\sum_i[\mathbf{E}_4^{-1}(\mathbf{q})]^{\mu\sigma}E_3^{\sigma i}(-\mathbf{q})u_i(\mathbf{q})\ . \tag{C2}$$

Further, since

$$\sum_{\mathbf{R},\mathbf{R}'}\sum_{i,j}u_i(\mathbf{R}')F_1^{ij}(\mathbf{R})u_j(\mathbf{R}+\mathbf{R}')=\sum_{\mathbf{q}}\sum_{i,j}u_i(\mathbf{q})E_1^{ij}(\mathbf{q})u_j(-\mathbf{q})\ ,$$

etc., from Eqs. (15) and (C2) we get

$$\beta\Delta F=\tfrac{1}{2}\sum_{\mathbf{q}}\sum_{i,j}u_i(\mathbf{q})D^{ij}(\mathbf{q})u_j(-\mathbf{q})$$

with the dynamical matrix $D(\mathbf{q})$ given by

$$\beta D^{ij}(\mathbf{q})=E_1^{ij}(\mathbf{q})-\sum_{\mu,\sigma=1}^{6}E_2^{i\mu}(\mathbf{q})[\mathbf{E}_4^{-1}(\mathbf{q})]^{\mu\sigma}E_3^{\sigma j}(\mathbf{q})\ . \tag{C3}$$

From Eq. (C3) it is clear that the dynamical matrix has two parts: (1) The first term is because of the displacements of the atoms. (2) The other because of the distortions of the Gaussian density distributions [Eq. (B1)].

To give explicit expressions for the $\mathbf{E}_i(\mathbf{q})$'s, it is convenient to switch back to the original indices (ij) from the Greek indices (μ) and write the related quantities $\boldsymbol{\varepsilon}_i(q)$'s as the Fourier transforms of $\mathbf{H}_i(\mathbf{R})$'s [Eqs. (11a)–(11c)]. Thus,

$$\varepsilon_1^{ij}(\mathbf{q})=\sum_{\mathbf{R}}H_1^{ij}(\mathbf{R})e^{i\mathbf{q}\cdot\mathbf{R}}\ ,$$

etc. Therefore, using Eqs. (11a)–(11c) and (A10) we get the results stated in Eqs. (20a)–(20c) of the text.

APPENDIX D: ELASTIC CONSTANTS

The elastic constants of a crystal can be calculated from the phonon dispersion relation in the limit $q\to0$. We calculate the velocities of sound (which are related to the elastic constants) from Eqs. (A18) and (20a)–(20c). In the limit of small q, we get

$$\varepsilon_1^{ij}(\mathbf{q})=\frac{-1}{\rho_0 v_{\text{cell}}}\sum_{\mathbf{G}(\neq0)}e^{-G^2/2\beta_0}\left[c(G)\left[q_iq_j-\tfrac{1}{2}q^2G_iG_j/\beta_0-\beta_0^{-1}(G_iq_j+G_jq_i)\sum_{m=1}^{3}G_mq_m\right]\right.$$
$$+\frac{dc(G)}{dG}\left[-\frac{G_iG_j}{\beta_0G}\sum_{m,n=1}^{3}G_mG_nq_mq_n+\frac{(G_iq_j+G_jq_i)}{G}\sum_{m=1}^{3}G_mq_m\right.$$
$$\left.+1/2\frac{q^2}{G}G_iG_j-1/2\frac{G_iG_j}{G^3}\sum_{m,n=1}^{3}G_mG_nq_mq_n\right]$$
$$\left.+\frac{d^2c(G)}{dG^2}\left[1/2\frac{G_iG_j}{G^2}\sum_{m,n=1}^{3}G_mG_nq_mq_n\right]\right]-\frac{c_0}{\rho_0v_{\text{cell}}}q_iq_j\ , \tag{D1a}$$

$$\varepsilon_2^{ijk}(\mathbf{q})=\frac{\sqrt{-1}}{4\beta_0\rho_0v_{\text{cell}}}\sum_{\mathbf{G}(\neq0)}e^{-G^2/2\beta_0}\left[c(G)\left[G_iG_jq_k+G_iG_kq_j+G_jG_kq_i-\beta_0^{-1}G_iG_jG_k\sum_{n=1}^{3}G_nq_n\right]\right.$$
$$\left.+\frac{dc(G)}{dG}\left[\frac{G_iG_jG_k}{G}\sum_{n=1}^{3}G_nq_n\right]\right]$$
$$=-\varepsilon_2^{ijk}(\mathbf{q})\ , \tag{D1b}$$

$$\varepsilon_4^{ijkn}(\mathbf{q})=-\tfrac{1}{4}(\delta_{in}\delta_{jk}+\delta_{ik}\delta_{jn})-\frac{1}{8\rho_0 v_{\text{cell}}}\sum_{\mathbf{G}(\neq 0)} e^{-G^2/2\beta_0}c(G)\frac{G_iG_jG_kG_n}{\beta_0^2}$$
$$+\frac{1}{4\rho_0 v_{\text{cell}}}(\delta_{ik}\delta_{jn}+\delta_{in}\delta_{jk})\sum_{\mathbf{G}(\neq 0)} e^{-G^2/2\beta_0}(G_i^2+G_j^2)/\beta_0+O(q^2)\ , \tag{D1c}$$

where δ_{ij} are the Kronecker δ functions and the subscripts on G and q denote the Cartesian components of the vectors $\mathbf{G}$ and $\mathbf{q}$. Equations (D1a)–(D1c) are used to evaluate the dynamical matrix (C3) for the wave-vector direction $\mathbf{q}/|\mathbf{q}|$. By diagonalizing the dynamical matrix for small $|\mathbf{q}|$, we calculate the frequencies of lattice vibration (longitudinal and transverse) and thus calculate the velocities of sound.

We illustrate the calculation of sound velocities in the (200) direction of the crystal using Eqs. (D1a)–(D1c). Since, in this direction, the dynamical matrix is diagonal, we can straightaway write the results for the longitudinal and transverse modes of vibration.

1. Longitudinal mode of vibration in the (200) direction

The element of dynamical matrix describing the longitudinal vibration has two parts: $D_l^u(\mathbf{q})$ and $D_l^\phi(\mathbf{q})$. For small q,

$$\beta D_l^u(\mathbf{q})=-\frac{q^2}{\rho_0 v_{\text{cell}}}\sum_{\mathbf{G}(\neq 0)} e^{-G^2/2\beta_0}\left[c(G)\left[1-\frac{5}{2}\frac{G_1^2}{\beta_0}\right]+\frac{dc(G)}{dG}\left[-\frac{G_1^4}{\beta_0 G}+\frac{5}{2}\frac{G_1^2}{G}-\frac{1}{2}\frac{G_1^4}{G^3}\right]\right.$$
$$\left.+\frac{d^2c(G)}{dG^2}\left[\frac{1}{2}\frac{G_1^4}{G^2}\right]\right]-\frac{q^2c_0}{\rho_0 v_{\text{cell}}} \tag{D2a}$$

is the contribution because of the displacements of the atoms and

$$\beta D_l^\phi(q)=\frac{(q^2/8)\left[(1/\beta_0\rho_0 v_{\text{cell}})\sum_{\mathbf{G}} e^{-G^2/2\beta_0}\{c(G)[3G_1^2-(G_1^4/\beta_0)]+[dc(G)/dG](G_1^4/G)\}\right]^2}{\left[1+(1/\rho_0 v_{\text{cell}})\sum_{\mathbf{G}} e^{-G^2/2\beta_0}c(G)(G_1^2/\beta_0)[1/4(G_1^2/\beta_0)-1]\right]} \tag{D2b}$$

is the contribution because of the distortion of the Gaussian density distributions. G_i's are the ith Cartesian components of $\mathbf{G}$.

2. Transverse modes of vibration in the (200) direction

In this case also, the relevant elements of the dynamical matrix have two parts, D_t^u and D_t^ϕ. For small q,

$$\beta D_t^u(\mathbf{q})=-\frac{q^2}{\rho_0 v_{\text{cell}}}\sum_{\mathbf{G}} e^{-G^2/\beta_0}\left[c(G)\left[-1/2\frac{G_2^2}{\beta_0}\right]+\frac{dc(G)}{dG}\left[-\frac{G_2^2G_3^2}{\beta_0 G}+\frac{G_2^2}{2G}-1/2\frac{G_2^2G_3^2}{G^3}\right]\right.$$
$$\left.+\frac{d^2c(G)}{dG^2}\left[1/2\frac{G_2^2G_3^2}{G^2}\right]\right] \tag{D3a}$$

is the contribution because of displacements of the atoms, and

$$\beta D_t^\phi(q)=\frac{-q^2\left[(1/\beta_0\rho_0 v_{\text{cell}})\sum_{\mathbf{G}} e^{-G^2/2\beta_0}\{c(G)[G_2^2-(G_2^2G_3^2/\beta_0)]+[dc(G)/dG](G_2^2G_3^2/G)\}\right]^2}{\left[-1-(1/\rho_0 v_{\text{cell}})\sum_{\mathbf{G}} e^{-G^2/2\beta_0}c(G)(G_2^2/\beta_0)[1/2(G_3^2/\beta_0)-1]\right]} \tag{D3b}$$

is the contribution because of the distortion of the Gaussian density distributions. The velocities of sound in the (200) direction are, therefore,

$$v_l=\frac{\sqrt{D_l^u(\mathbf{q})+D_l^\phi(\mathbf{q})}}{\sqrt{M}q}\quad\text{(longitudinal)}\ , \tag{D4a}$$

$$v_t=\frac{\sqrt{D_t^u(\mathbf{q})+D_t^\phi(\mathbf{q})}}{\sqrt{M}q}\quad\text{(transverse)}\ , \tag{D4b}$$

where M is the atomic mass.

*Present address: School of Physics, University of Hyderabad, Hyderabad 500 134, Andhra Pradesh, India.
†Also at the Jawaharlal Nehru Centre for Advanced Scientific Research, I.I.Sc. campus, Bangalore 560 012, India.
‡Address: Joseph Henry Laboratory of Physics, Jadwin Hall, Princeton University, Princeton, NJ 08542.

[1]M. Born and K Huang, *Dynamical Theory of Crystal Lattices* (Clarendon Press, Oxford, 1954).
[2]E. G. Brovman, and Yu. M. Kagan, in *Dynamical Properties of Solids,* edited by G. K. Horton and A. A. Maradudin (North-Holland, Amsterdam, 1974), Vol. 1.
[3]M. L. Klein and T. R. Koehler, in *Rare Gas Solids,* edited by M. L. Klein and J. A. Venables (Academic, New York, 1976), Vol. 1.
[4]At temperatures above one-third of the melting temperature, the ratio of root-mean-square amplitude of vibration to the nearest atomic distance is more than 0.06 and less than 0.1 [M. L. Klein, G. K. Horton, and J. L. Feldman, Phys. Rev. **184**, 968 (1969)].
[5]H. Horner, in *Dynamical Properties of Solids,* Ref. 2.
[6]E. R. Cowley and G. K. Horton, Phys. Rev. Lett. **58**, 789 (1987).
[7]T. V. Ramakrishnan and M. Yussouff, Phys. Rev. B **19**, 2775 (1979).
[8]A. D. J. Haymet and D. W. Oxtoby, J. Chem. Phys. **74**, 2559 (1981). For a recent review and other references, see D. W. Oxtoby, *Liquids, Freezing and the Glass Transition,* 1989 Les Houches Lectures (North-Holland, Amsterdam, 1990).
[9]There has been some recent work [J. L. Barrat, J. P. Hansen, and G. Pastore, Phys. Rev. Lett. **58**, 2075 (1987)] on the approximate calculation of three-body corelation functions.
[10]P. Tarazona, Mol. Phys. **52**, 81 (1984).
[11]W. A. Curtin and N. W. Ashcroft, Phys. Rev. A **32**, 2909 (1985); Phys. Rev. Lett. **56**, 2775 (1986).
[12]M. Baus, Mol. Phys. **53**, 183 (1984).
[13]G. Jones and U. Mohanty, Mol. Phys. **54**, 1241 (1985).
[14]A partial motivation [S. Sachdev and D. R. Nelson, Phys. Rev. B **32**, 4592 (1985)] for Eq. (4) can be obtained as follows: Consider the self-consistency equation (3) for $\rho(\mathbf{r})$. Since $e^{i\mathbf{G}\cdot\mathbf{R}}=1$, for any $\mathbf{G}$, $\rho(\mathbf{r})$ has a maximum whenever $\mathbf{r}=\mathbf{R}$. By expanding $e^{i\mathbf{G}\cdot\mathbf{r}}$ in Eq. (3) about $\mathbf{r}=\mathbf{R}$, it is easy to see that, in the vicinity of $\mathbf{r}=\mathbf{R}$, $\rho(\mathbf{r})$ has the Gaussian form as in Eq. (4). Another way of motivating (4) is to note that its Fourier coefficients are $\mu_{\mathbf{G}} \propto e^{-a^2G^2/4\alpha_0}$. Thus, the Debye-Waller factor $|\mu_{\mathbf{G}}|^2$ corresponding to (4) has the form $\exp(-\frac{1}{2}G^2U^2)$, where $U^2=a^2/\alpha_0$, which is a constant independent of $\mathbf{G}$. Several calculations of the $\mathbf{G}$ dependence of $|\mu_{\mathbf{G}}|$ that satisfy the self-consistent equation (3) in a variety of contexts (Refs. 7 and 8) have shown that U is almost constant beyond the first few reciprocal lattice shells, and its deviation from the asymptotic value for those first shells is not more than 10%. Thus, the Gaussian parametric form (4) is quite reasonable.
[15]O. G. Peterson, D. N. Batchelder, and R. D. Simmons, Philos. Mag. **12**, 1193 (1965); Phys. Rev. **150**, 703 (1966).
[16]By the entropic part we mean the part that arises because of the ln term in the free-energy functional. Of course, some entropic contributions are also included in the direct correlation function which we use as an effective potential.
[17]T. V. Ramakrishnan, Pramana **22**, 365 (1984); H. R. Krishnamurthy and T. V. Ramakrishnan (unpublished).
[18]M. V. Jarić and U. Mohanty [Phys. Rev. B **37**, 4441 (1988)] have used the Gaussian form for the local density in the context of the density-fucntional theory for the strain energy and the elastic constants of a crystal (Ref. 17). Since ours is the first study that uses the density-functional theory of freezing to obtain the phonon spectra of crystalline solids, we feel justified in using the simplest RY density functional and the simplest approximation for $\rho(\mathbf{r})$ namely, the Gaussian form.
[19]This is a consistent assumption. In principle, this α_{ij} should be calculated self-consistently. Since the free energy should be a minimum with respect to α_{ij}, it should contain no term linear in α_{ij}. We retain, in our calculation, terms up to quadratic order in α_{ij} and calculate them by minimizing the free energy, whence α_{ij} are proportional to $|\mathbf{u}|$ [Eq. (16)].
[20]A. A. Maradudin, *Dynamical Properties of Solids,* Ref. 2.
[21]A. A. Maradudin, E. W. Montrol, G. H. Weiss, and I. P. Ipatova, *Solid State Physics,* 2nd Ed. (Academic, New York, 1971), Vol. 3, p. 200.
[22]P. J. Hunter and J. S. Rowlinson, in *Simple Dense Fluids,* edited by H. L. Frisch and Z. W. Salsburg (Academic, New York, 1968).
[23]D. I. Page (unpublished).
[24]J. L. Yarnell, M. J. Katz, R. G. Wenzel, and S. H. Koenig, Phys. Rev. A **7**, 2130 (1973).
[25]L. Verlet, Phys. Rev. **165**, 201 (1967).
[26]W. H. Press, B. P. Flannery, S. A. Teukolsky, and W. T. Vetterling, *Numerical Recipes* (Cambridge University, Cambridge, 1987).
[27]S. Goldman, J. Phys. Chem. **83**, 3033 (1979).
[28]J. M. H. Levelt, Physica **26**, 361 (1960).
[29]C. Marshall, B. B. Laird, and A. D. J. Haymet, Chem. Phys. Lett. **122**, 320 (1985).
[30]J. J. Nicolas, K. E. Gubbins, W. B. Streett, and D. J. Tildesley, Mol. Phys. **37**, 1429 (1979).
[31]H. R. Moeller and C. F. Squire, Phys. Rev. **151**, 689 (1966).
[32]J. Eckert and R. W. Youngblood, Phys. Rev. B **34**, 2770 (1986).
[33]Y. Fujii, N. A. Lurie, R. Pynn, and G. Shirane, Phys. Rev. B **10**, 3647 (1974).
[34]W. A. Curtin, Phys. Rev. B **39**, 6775 (1989).
[35]B. B. Laird, J. D. McCoy, and A. D. J. Haymet, J. Chem. Phys. **87**, 5449 (1987).
[36]A. R. Denton and N. W. Ashcroft, Phys. Rev. A **39**, 4701 (1989).
[37]A. de Kuijper, W. L. Vos, J.-L. Barrat, J.-P. Hansen, and J. A. Schouten, J. Chem. Phys. **93**, 5187 (1990).
[38]G. Zerah and J.-P. Hansen, J. Chem. Phys. **84**, 2336 (1986).
[39]C. Ebner, H. R. Krishnamurthy, and R. Pandit, Phys. Rev. A **43**, 4355 (1991).
[40]S. Sengupta and H. R. Krishnamurthy (unpublished).